



Green
Chemistry

**Recent Advances in Selectively Catalytic
Hydrodeoxygenation of Lignin-derived Oxygenates to
Arenes**

Journal:	<i>Green Chemistry</i>
Manuscript ID	GC-TRV-08-2019-002762.R1
Article Type:	Tutorial Review
Date Submitted by the Author:	20-Dec-2019
Complete List of Authors:	Zhang, Jiangho; Washington State University College of Engineering and Architecture, The Gene and Linda Voiland School of Chemical Engineering and Bioengineering Sun, Junming; Washington State University, The Gene & Linda Voiland School of Chemical Engineering and Bioengineering Wang, Yong; Pacific Northwest National Laboratory, Institute for Integrated Catalysis

SCHOLARONE™
Manuscripts

ARTICLE

Received 00th January 20xx,
Accepted 00th January 20xx

DOI: 10.1039/x0xx00000x

Recent Advances in Selectively Catalytic Hydrodeoxygenation of Lignin-derived Oxygenates to Arenes

Jianghao Zhang,^a Junming Sun^{*a} and Yong Wang^{*a,b}

Utilization of the lignin-derived compounds is an important part of biomass valorization. One promising way to achieve this goal is to reduce/eliminate the oxygen content via hydrodeoxygenation (HDO), producing valuable fuels and chemicals. However, most of HDO catalysts are not selective in arene production, having the tendency to saturate aromatic rings and thus consuming excess hydrogen. In this review, we summarize the recent advances in catalysts for phenol HDO and understanding of reaction mechanisms involved, aiming to provide a perspective for developing highly efficient HDO catalysts. In particular, we first present an overview of HDO of phenolics, including the challenges in selective removal of oxygen without saturating the aromatic ring. Then we focus on the characteristics of four types of HDO catalysts, i.e. sulfides, base metals (oxides), noble-metal-based catalysts, and carbides/nitrides/phosphides, and the potential approaches to improve their arene selectivity. Finally, we attempt to generate a correlation between catalysts' oxophilicity and the performances in the HDO of phenolics, which can potentially serve as the basis for the design of selective HDO catalysts.

1 Introduction

With more stringent environmental regulations and the concerns of depleting fossil resource¹, various unconventional energy carriers (e.g. shale gas, solar, biomass, etc.) have been investigated and developed²⁻⁴. Among these potential alternatives, biomass is the only renewable organic carbon resource in nature.⁵ Due to its abundance and inedibility, lignocellulosic biomass, comparing with other forms of biomass such as algae and vegetable oil, has attracted greatest interest in both industry and academia for the production of biofuels⁶⁻⁸. Lignocellulosic biomass is composed of three major components: cellulose, hemicellulose and lignin.⁹ Unlike the other two components, lignin is the most recalcitrant biopolymer to protect the plant tissue from mechanical stress and microbial attack¹⁰. However, lignin is underutilized in most of the current refinery processes¹¹, e.g., it usually serves as the low-value solid fuel burned to generate power for maintaining the biorefinery process¹² or even is treated as waste in pulp and paper plants¹³. Valorization of lignin has thus been attracting attentions given that it is the most abundant source for

renewable aromatic compounds¹⁴, which makes up 15-30% by weight¹⁵⁻¹⁷ and up to 40% by energy^{9, 16} of lignocellulose.

One potential process to valorize lignin is to convert it into fuel components that are compatible with the petroleum-derived fuels^{18, 19}. Since lignin is an amorphous macropolymer with three-dimensional structure which is primarily composed of monolignols with ether and C-C linkage⁵, the indispensable step to upgrade lignin to fuel is depolymerization²⁰. Depolymerization of lignin mainly produces aromatic oxygenates such as anisole and guaiacol¹³. The feasibility of directly mixing the aromatic oxygenates, such as anisole and guaiacol, with gasoline for spark ignition engine has been investigated. Although blending 10 vol.% of these oxygenates with Euro95 fuel showed no significant differences in thermal efficiency, the anti-knock quality was negatively impacted²¹. Additionally, these oxygenates decrease the volatility and increase the viscosity of the fuels²². Therefore, oxygen removal is preferred to resolve the above problems, as well as to increase the energy density²³.

Oxygen removal from phenols can be achieved with different approaches such as deoxygenation using a variety of hydrogen donors²⁴⁻²⁷, deoxygenation through resin-bound aryl triflate²⁸, enzymatic conversion²⁹, etc. Among those, hydrodeoxygenation (HDO) is considered as one of the most viable processes^{6, 30}. In a HDO process, aromatic oxygenates are exposed to hydrogen atmosphere in the presence of catalyst at a moderate temperature usually between 200 °C to 500 °C where the oxygen in the substrates is removed in the form of water and/or other small oxygenates (CO_x, methanol, etc.)³¹⁻³³.

^aThe Gene & Linda Voiland School of Chemical Engineering and Bioengineering, Washington State University, Pullman WA, United States of America 99164. E-mail: Junming.sun@wsu.edu

^bInstitute for Integrated Catalysis, Pacific Northwest National Laboratory, Richland, WA, United States of America 99352. E-mail: yong.wang@pnnl.gov

† Footnotes relating to the title and/or authors should appear here.

Electronic Supplementary Information (ESI) available: [details of any supplementary information available should be included here]. See DOI: 10.1039/x0xx00000x

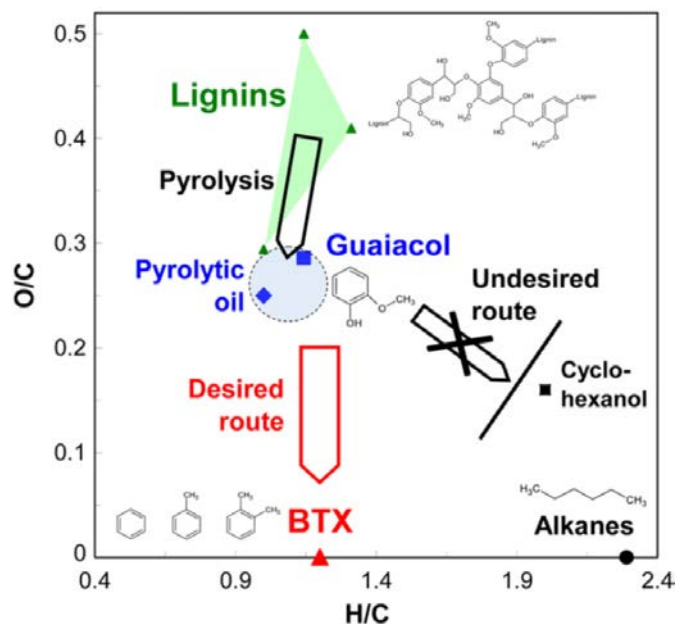


Figure 1. Van Krevelen diagram of hydrotreatment of lignin and lignin-derived phenols. Reprinted from Olcese et al.,³⁷ Copyright (2012), with permission from Elsevier.

Two typical reaction pathways are widely accepted in the catalytic HDO of aromatic oxygenates: (1) hydrogenation-deoxygenation (HYD) to ring-saturated hydrocarbons and (2) direct deoxygenation (DDO) via C-O bond cleavage to aromatic hydrocarbons³⁴. Due to the high bond dissociation energy (BDE) of C_{aromatic}-O bond^{25, 35}, DDO route usually has a higher barrier and the HYD route with its ring-saturated products dominate

over most of the sulfur-free catalysts. However, preserving the aromatic ring during selective removal of oxygen is preferred³⁶ in order to minimize hydrogen consumption and to produce a gasoline blending stock with higher octane number (higher anti-knock quality)²². The Van Krevelen diagram (plotted for hydrotreatment of lignin and phenols (Figure 1) further highlighted the desirable DDO pathway to produce benzene, toluene, xylene (BTX) from lignin-derived pyrolytic oil³⁷. In the U.S. Department of Energy's Multi-Year Program Plan 2016 for Bioenergy Technologies Office, oxygen removal strategies and hydrotreating catalysts that are highly selective to desired end products are counted as the main challenges and barriers in biomass conversion³⁸. Therefore, great efforts have been devoted in selective hydrodeoxygenation of phenols, and indeed a few catalysts with high arene selectivity have been developed^{39, 40}.

Some excellent reviews have provided extensive summary of the precedent understanding of HDO reaction^{41, 42}, historical development²², as well as recent advance of this hydrotreating process^{43, 44}, etc. Certain publications focused on the HDO of lignin-derived phenols^{7, 13, 18, 45}, and the reaction parameters that influence the product selectivity⁴⁶. To our best knowledge, no review has been reported focusing on the catalyst developments for selective HDO to arenes. Herein, we summarize the recent advances in developing selective HDO catalysts, in an attempt to provide the deep insights into the reaction mechanism involved as well as perspectives for the design of highly efficient HDO catalysts toward arene production.

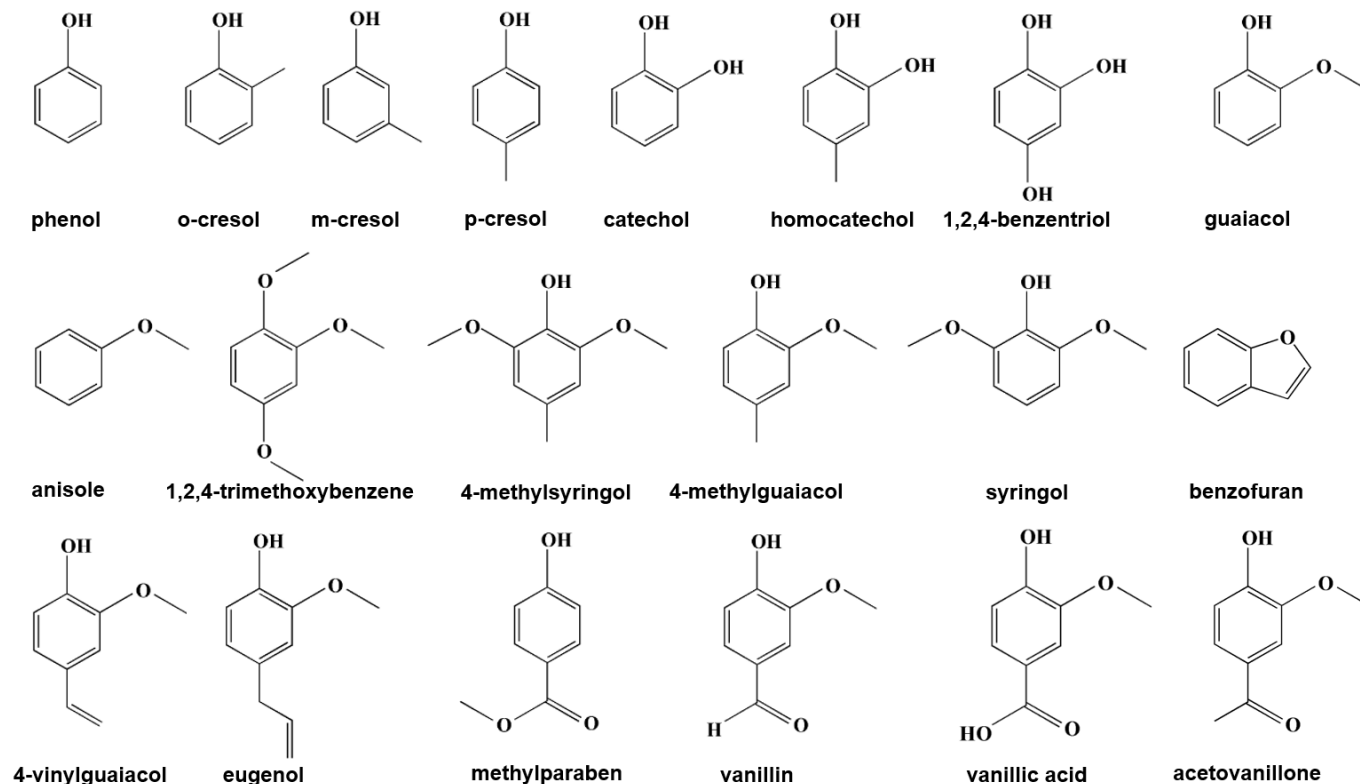


Figure 2. The selected aromatic oxygenates derived from pyrolysis of lignin⁴⁹.

2 Structure and Properties of Lignin-derived Oxygenates

Lignin is randomly polymerized with three primary monolignols: coumaryl, coniferyl, and sinapyl alcohols, forming the recalcitrant phenolic macromolecules⁴⁷. Currently, the depolymerization of lignin are mainly processed through thermochemical approaches such as pyrolysis, oxidation, hydrotreating and hydrolysis. Other than that, biological and electrochemical methods have been also investigated^{47, 48}. The composition of depolymerized products is highly dependent on the process employed. Pyrolysis produces pyrolytic oil consisting of phenolic compounds, as well as certain amounts of gasified compounds and char⁴⁹. Hydrotreating converts lignin to liquid oil including phenols, which may be further *in-situ* deoxygenated to hydrocarbons in the presence of catalyst²⁰. Oxidation process produces phenols and aromatic aldehydes⁵⁰⁻⁵². The details on the depolymerization of lignin have been well summarized in several recent literature^{12, 47, 51, 53, 54}. Regardless, these lignin depolymerization processes mainly result in the production of an arsenal of aromatic oxygenates (Figure 2). Majority of oxygen-containing functional groups in these aromatics could be classified as hydroxyl ($C_{\text{aromatic}}\text{-OH}$ bond) and ether ($C_{\text{aromatic}}\text{-O-C}$ bond). Table 1 displays the BDE of $C_{\text{aromatic}}\text{-OH}$ and $C_{\text{aromatic}}\text{-O-C}$ bonds in the representative molecules. It's clear that the BDE sequence follows the order of $C_{\text{aromatic}}\text{-OH} > C_{\text{aromatic}}\text{-OC} > C_{\text{aromatic}}\text{-O-C}$. In addition, it has been demonstrated that, over Ni catalyst, activation energy of hydrogenolysis of ether bond can be well correlated with the BDE¹⁷. Most of the catalysts cleave the weakest $C_{\text{aromatic}}\text{-O-C}$ bond forming the strongest $C_{\text{aromatic}}\text{-OH}$ bond in hydrogen atmosphere^{55, 56}. Therefore, the main challenge in selective HDO of phenolic oxygenates is the removal of oxygen in the $C_{\text{aromatic}}\text{-OH}$ group, with phenol as the simplest representative.

Table 1. The bond dissociation energy (BDE) of representative lignin-derived compounds^{35, 57}.

Molecule	Bond	BDE (kJ/mol)
Anisole	$C_6H_5\text{-OCH}_3$	418.8 ± 5.9
	$C_6H_5\text{O-CH}_3$	263.2 ± 4.2
Guaiacol	$\text{HOC}_6H_5\text{-OCH}_3$	379.1
	$\text{HOC}_6H_5\text{O-CH}_3$	235.6
Ethyl phenyl ether	$C_6H_5\text{-OC}_2H_5$	416.7 ± 5.4
	$C_6H_5\text{O-C}_2H_5$	269.0 ± 4.8
Phenol	$C_6H_5\text{-OH}$	463.6 ± 4.2
Cresol	$\text{CH}_3C_6H_5\text{-OH}$	443

3 Overview to the HDO of Lignin-derived Aromatic Oxygenates

A detailed reaction network for the conversion of representative phenolic compounds was summarized by Runnebaum et al.⁵⁸ based on the HDO reaction over $\text{Pt}/\gamma\text{-Al}_2\text{O}_3$ catalysts (Figure 3). In this hydroprocessing with the aim of oxygen removal, deoxygenation is accompanied with other reactions such as acid-catalyzed transalkylation, hydrogenolysis of ether bond (e.g. cleavage of $C_6H_5\text{O-CH}_3$ bond) and hydrogenation of the aromatic ring. Three groups of products are obtained: aromatic hydrocarbons, aliphatic hydrocarbons and aliphatic oxygenates. The relations between the formation of different products with extent of oxygen removal, as well as the amount of H_2 consumption are displayed in Figure 4 where phenol HDO is taken as an example. Producing benzene shows the lowest H_2 consumption and highest oxygen removal ratio to increase the energy density. Moreover, arenes have much higher octane number²², which can also be interpreted as better anti-knock quality than that of aliphatic hydrocarbon. Therefore, selective production of arenes from aromatic oxygenates is desired in HDO process.

From thermodynamics point of view, preservation of the aromatic ring is only favored in a limited range of reaction conditions. Olcese et al.³⁷ calculated the equilibrium from guaiacol and hydrogen at 1 atmospheric pressure. By determining the variation of free Gibbs energy at different temperatures, it is proposed that the preservation of the aromatic ring started to be favored at above 427 °C, where coke tends to form. Baddour et al.⁵⁹ also calculated the equilibrium constant for cyclohexane – benzene – hydrogen system as a function of temperature (Figure 5a), and the change of equilibrated product distribution by variation of pressure at 300 °C is shown in Figure 5b. The results suggest that only at low hydrogen pressure and high temperature the formation of aromatic hydrocarbon is favorable. This result is consistent with the study by Yohe et al.¹⁵ that decreasing the hydrogen pressure from 342 psi to 14.2 psi dramatically increases the arene selectivity from near 0% to above 90% and by Rensel et al.⁶⁰ that increasing the temperature from 300 °C to 400 °C promotes the arene selectivity from 28% to 90%.

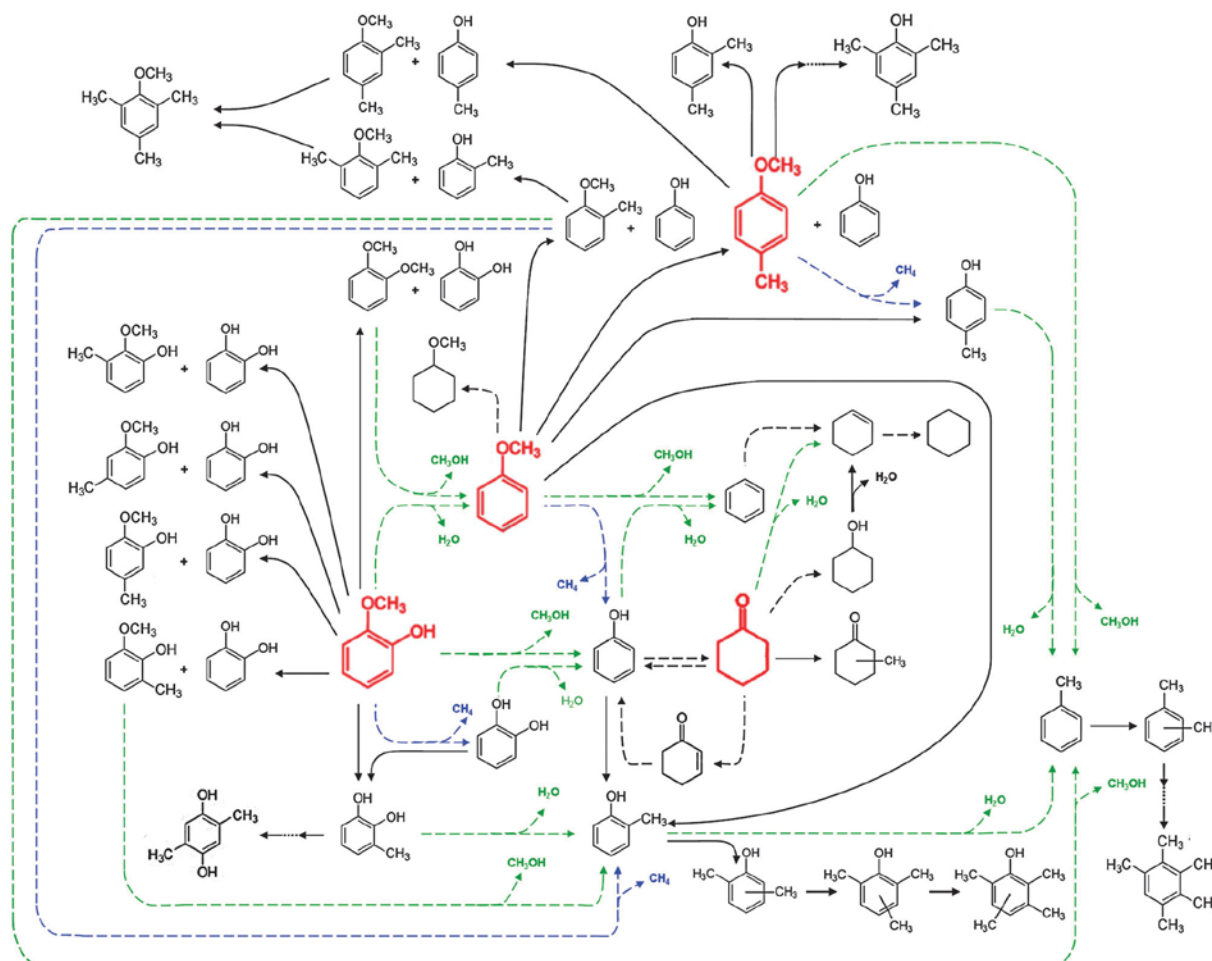


Figure 3. Reaction network in the conversion of lignin-derived compounds catalyzed by Pt/ γ -Al₂O₃ at 300 °C and 140 kPa. Deoxygenation, hydrogenolysis, and hydrogenation (or dehydrogenation) reactions are represented by dashed green, blue, and black arrows, respectively. Transalkylation reactions are represented by solid black arrows. H₂ as a reactant is omitted for simplicity. Reprinted from Runnebaum et al.⁵⁸

In general, three reaction pathways have been proposed in the HDO of phenols: direct C–O bond cleavage, direct aromatic ring hydrogenation, and keto-enol tautomerization (isomerization of phenol to form cyclohexadienone followed by hydrogenation of C=C and C=O bonds)⁶¹, as summarized in Figure 6 for the case

of phenol. Although each reaction pathway can lead to benzene formation, the productivity varies significantly at same reaction condition. At high H₂ partial pressures, direct ring saturation pathway is not able to produce benzene because the dehydrogenation of cyclohexene to benzene is thermodynamically unfavorable, whereas direct C–O bond cleavage forms benzene as a primary product in this pathway. Also, high H₂ pressure can enhance the hydrogenation of intermediates in tautomerization pathway, resulting in decreased benzene selectivity. Our recent work further demonstrated that over Fe-based catalysts, tautomerization pathway is the major cause of ring saturation in the liquid-phase HDO of phenol at high H₂ pressures (above 10 bar)⁶². At low H₂ pressure where dehydrogenation of cyclohexene is no longer the thermodynamic bottleneck, both direct ring saturation pathway and tautomerization pathway are able to yield benzene with high selectivity, as demonstrated by previous studies^{63, 64}. Based on the reaction network, an efficient methodology to selectively produce arene should be realized by kinetically enhancing the direct C–O bond cleavage activity and/or inhibiting the ring hydrogenation steps.

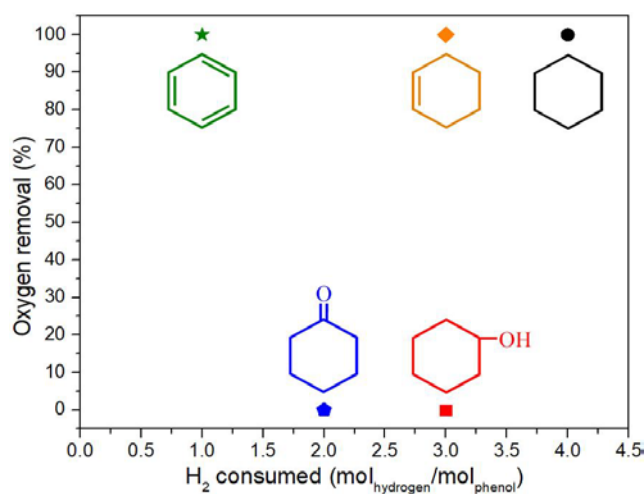


Figure 4. Oxygen removal and H₂ consumption ratio as a function of yielding different products in the HDO of phenol.

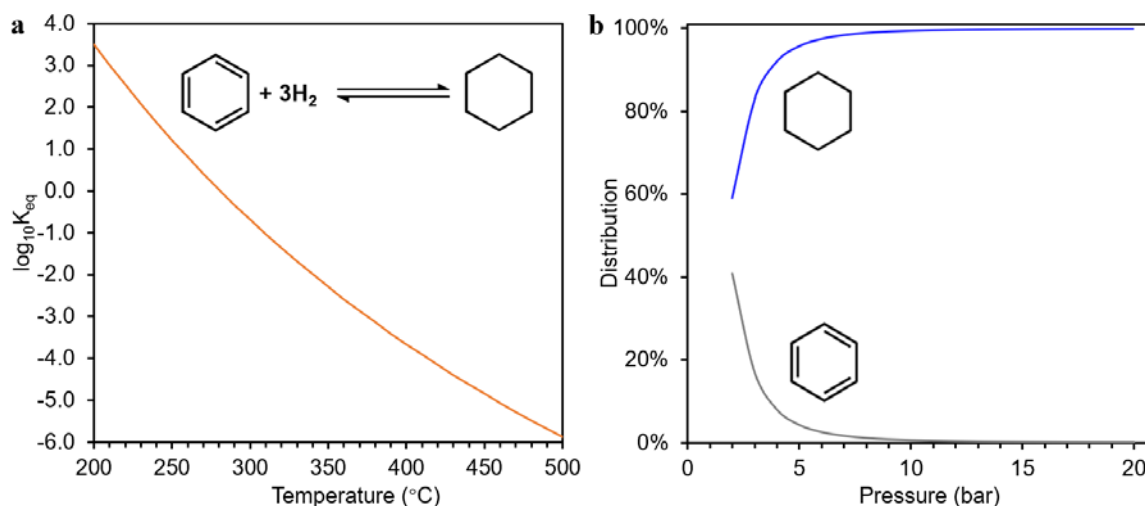


Figure 5. Thermodynamic equilibrium for the reaction of benzene and hydrogen to produce cyclohexane plotted as a function of temperature (a) and total pressure (b).

Life time is one of the key parameters to evaluate a catalyst. Extending the catalyst life time always relies on the fundamental understanding of the deactivation mechanism. Given the complex composition of products from depolymerization of lignin^{49, 65}, the deactivation mechanisms may vary depending on impurities, reacting conditions and catalysts. One common cause for the deactivation of HDO catalyst is the block of active site by coke or strongly adsorbed species. Coking, one of the major challenges for HDO reaction¹³, has been reported during the HDO on sulfides^{66, 67}, noble metals⁶⁸, catalysts with zeolite as support⁶⁹, etc. Another reason for the deactivation is surface phase transformation of catalyst during the HDO. For example, MoS₂⁷⁰ and Fe⁷¹ could be oxidized in the presence of water and other oxygenates, leading to the less active phase on surface. The third deactivation mechanism is the poisoning of active site by the impurities. For example, alkali metals had been reported to poison the Ni-based and sulfide catalysts^{72, 73}. The deactivation can also be caused by sintering that decreases the amount of active sites⁷⁴. Several previous publications have well reviewed the deactivation mechanisms and potential regeneration of catalysts, the reader is referred to these literatures^{67, 75, 76} for in-depth discussion.

4. Selective HDO of Lignin-derived Aromatic Oxygenates

Selective HDO of aromatic oxygenates has been extensively studied to produce arenes in both vapor-phase and liquid-phase conditions. The developed catalysts for HDO of phenolics can be classified into four categories: 1) metal sulfides; 2) base metals (oxides); 3) noble-metal-based catalysts; and 4) metal carbides, nitrides and phosphides.

4.1 Metal sulfide catalysts

The sulfided NiMo/Al₂O₃ and CoMo/Al₂O₃ catalysts were initially applied in commercial hydrotreatment such as hydrodesulfurization (HDS) and hydrodenitrogenation (HDN) in petroleum refineries^{70, 77}. With the inspiration of the similarity between the above processes and HDO, these sulfide catalysts have been also explored in HDO reactions. In these sulfides, CoMoS and NiMoS serve as the active phase. Several models have been proposed to interpret the catalytic performance of Mo-based sulfide including adsorption geometry⁷⁸, "rim-edge" model⁷⁹, sulfur vacancies⁸⁰ etc.

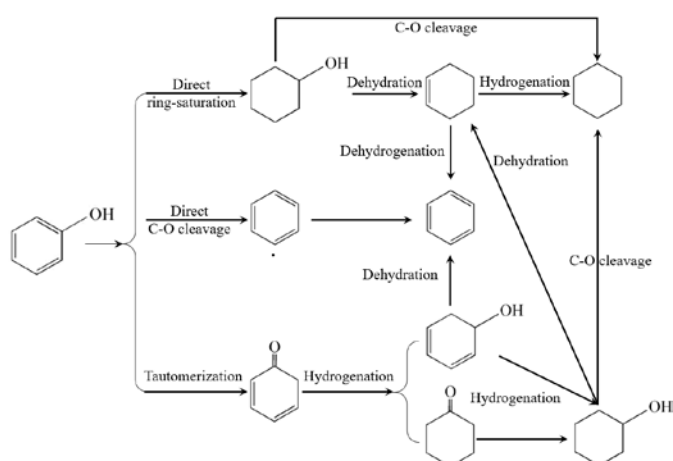


Figure 6. The proposed reaction pathways for HDO of phenol. Adapted from Zhang et al.⁶² Copyright (2020), with permission from Elsevier.

4.1.1 Proposed approaches to control the arene selectivity of sulfide catalyst

Adsorption geometry is proposed to influence the selectivity of hydrogenolysis and hydrogenation in HDS reaction: planar adsorption configuration favors the hydrogenation whereas perpendicular one favors hydrogenolysis as shown in Figure 7. Hensen et al.⁸¹ employed different supports for MoS₂ yielding distinct degree of average stacking. With a higher degree of stacking, the fraction of MoS₂ layers not directly attached to the support increased, leading to a favorable π -complexation with aromatics⁸¹. Conversely, a lower stacking degree favors perpendicular adsorption through S atom⁸¹, and consequently increases the hydrogenolysis selectivity in HDS. This model was also proposed in HDO⁸². Another DFT calculation shows the perpendicular geometry of guaiacol and phenol over CoMoS₂ and MoS₂ leads to adsorption via OH functional group being the most stable mode, which contributes to the dominant DDO reaction pathway to arene⁷⁸.

The “rim-edge” model, proposed in HDS of dibenzothiophene (DBT)⁸³, describes a stack of several layers of sulfide, where top surface of the disc is inert basal plane, the top and bottom layers are associated with rim sites and the sandwiched layers are edge ones. In this particular model, hydrogenation of aromatic ring is proposed to occur predominately on rim sites for DBT whereas hydrogenolysis takes place on both sites⁸³. This difference can be attributed to the fact that rim sites display higher coordinative unsaturation that facilitates interaction with aromatic ring. Since the relative fractions of the two sites depend on the number of the stacking layers, the MoS₂ with different stacking layers results in different hydrogenolysis selectivities. Wang et al.⁷⁹ synthesized MoS₂ with different average stacking layers for HDO of p-cresol, and confirmed the “rim-edge” model by the morphology-selectivity relationship showing that highest selectivity was achieved on the catalyst with largest number of stacking layers.

However, several reports cannot be fully interpreted by the above “rim-edge” model. The aforementioned study by Hensen et al.⁸¹ showed the seemingly opposite trend against “rim-edge” model about stacking degree and catalytic selectivity. Yang et al.⁸⁴ also showed that the MoS₂ with lowest stacking degree displayed minimum ring saturation whereas the most severe saturation happened over a moderate stacking. It should be

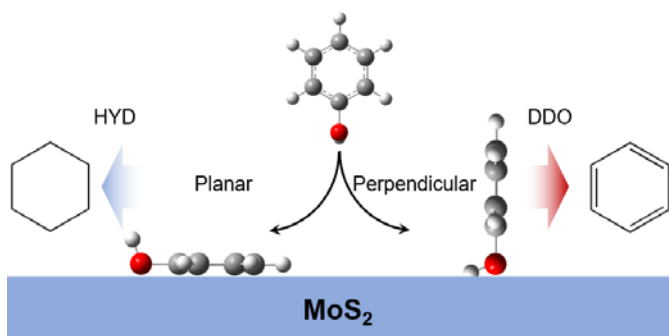


Figure 7. Illustration about adsorption geometry influences the reaction pathway and product distribution.

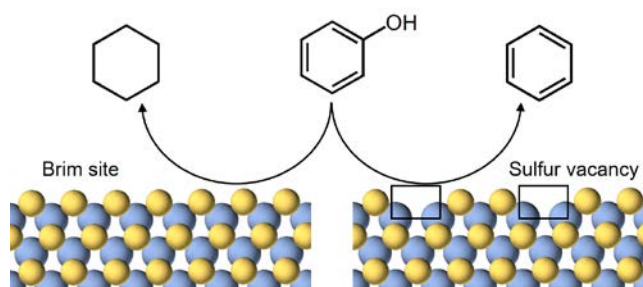


Figure 8. Different pathways may occur on brim site and sulfur vacancy during the HDO of phenol.

noted that the range of average stacking layer in Hensen’s report⁸¹ is 1.4-2.5, while the range in “rim-edge” model study⁸³ is 3.1-15.2. Therefore, it’s possible that inverse volcano curve may exist such that when the number of stacking layer increases from 1 to ~3.1, the adsorption configuration gradually switches to a planar mode which favors ring saturation, while further increasing the stacking to a higher number (where “rim-edge” model applies) provides more edge sites to enhance the hydrogenolysis. This explanation can also fit Yang’s report⁸⁴ well (MoS₂ with 1.8 and 57 stacking layer number both showed lower saturation to the ring than that of 9).

Another model for sulfide catalysts consists of sulfur vacancies and brim sites⁸⁰ as shown in Figure 8. In this model, the vacancies act as selective deoxygenation active sites while the brim sites hydrogenate the aromatic ring. Therefore, increasing the amount of sulfur vacancies on the surface promotes both the activity and arene selectivity, which can be achieved by adding Co or Ni since they weaken the sulfur-metal bond at the sites where the Co and Ni are anchored and promote the sulfur elimination⁸⁵. In the HDO reaction, the phenols are adsorbed with η_1 mode⁸⁶ (adsorption through O atom) onto the vacancies, followed by the C-O bond cleavage. The brim site located near the edge of the basal plane is proposed to catalyze the hydrogenation. Over the brim site, it was also proposed that the η_6 adsorption (adsorption through the aromatic ring) contributes to the hydrogenation of aromatic ring⁸⁰, as referenced from the adsorption geometry model. Consistent with this model, the sulfur vacancies were also found to promote activity in another novel work, showing monolayer Co-MoS₂ catalyst displayed high activity even at 180 °C⁴⁰.

4.1.2 Selective metal sulfide catalysts

In terms of catalytic performances, sulfides are by far the most reported catalysts showing high arene selectivity (Table 2). Victoria et al.⁸⁷ tested a commercial MoS₂ for HDO of cresol and identified two primary reactions, i.e. C-O bond cleavage to yield toluene and ring saturation followed by dehydration to form cyclohexene. The MoS₂ catalyst achieved 73% arene selectivity at 325 °C and 41 bar pressure. Wang et al.⁷⁹ found that the surfactants involved in the synthesis influence the arene selectivity of MoS₂ catalysts. Specifically, hydrothermal method was employed for the synthesis in the presence of different surfactants: hexadecyltrimethylammonium bromide (CT), polyvinylpyrrolidone (PV), and sodium lauryl benzenesulfate (DB). It was found that different types of surfactants adjusted

the stacking degree of the MoS₂ layers, and that PV led to the highest degree of stacking. As a result from rim-edge model (the range of stacking layer in this study is 3.7-4.9), MoS₂ derived from PV surfactant displayed a much higher arene selectivity (> 90%) than other Mo sulfides investigated in HDO of cresol at 300 °C and 40 bar. Besides the influences from synthesis method, the effect of water generated in the HDO reaction was also investigated⁸⁸. The presence of water was found to slightly improve the arene selectivity from 74.6% to 88.0% at 275 °C and

40 bar. The adsorbed water was proposed to dissociate to form Mo-OH group which perturbs the electron pair of oxygen in phenols, leading to facilitated C-O bond cleavage. Meanwhile, the η⁶ adsorption of aromatic ring (contributing to ring hydrogenation) which requires at least two neighboring S vacant sites was also found to be inhibited by the adsorbed water occupying certain amount of the S vacancies. Note that, the stability of the catalyst was negatively impacted by the co-fed water due to the severe loss of S on the active sites⁸⁸.

Table 2. Catalytic performances of sulfides with high arene selectivity in the HDO of aromatic oxygenates.

Catalyst	Reaction condition			Substrate	Conv. (%)	S _{arene} (%)	Note	Ref
	T(°C)	P (bar)	Solvent/Reactor ^a					
Mo-S	325	41	Decalin/b	Cresol	24	73	-	87
Mo-S	300	40	Dodecane/b	Cresol	40.4	74.4	hexadecyltrimethylammonium bromide (CTAB),	79
Mo-S-CT	300	40	Dodecane/b	Cresol	98.8	76.1	polyvinylpyrrolidone (PVP)	79
Mo-S-PV	300	40	Dodecane/b	Cresol	90.6	92.9	-	79
Mo-S	275	40	Hexadecane/b	Cresol	33.3	74.3	-	89
Mo-S	300	40	Dodecane/b	Cresol	67	74.1	-	90
Mo-S 1:1	275	40	Dodecane/b	Cresol	95.4	88	water to cresol ratio	88
Mo-S 0.5:1	275	40	Dodecane/b	Cresol	96.7	83.3	water to cresol ratio	88
Mo-S 1.25:1	275	40	Dodecane/b	Cresol	73.7	85.2	water to cresol ratio	88
Mo-S	300	30	Decalin/b	Cresol	25.8	94	-	40
^F Mo-S	300	30	Decalin/b	Cresol	69.6	87.2	F: few layer	40
^S Mo-S	300	30	Decalin/b	Cresol	98.7	83.1	S: single layer	40
Co- ^S Mo-S	300	30	Decalin/b	Cresol	83.6	99.2	-	40
Co-Mo-S	300	40	Decalin/b	Phenol	100	100	-	91
Co-Mo-S	300	40	Decalin/b	Cresol	100	100	-	91
Co-Mo-S-A-0.2	350	28	Decane/b	Phenol	98.2	80.3	A: amorphous	92
Co-Mo-S-A-0.6	350	28	Decane/b	Phenol	97.9	75.9	Number: Co ratio	92
Mo-S	275	40	Dodecane/b	Cresol	42	80.5	-	93
Co-Mo-S-0.1	275	40	Dodecane/b	Cresol	83.6	84.9	Number: Co/Mo mole ratio	93
Co-Mo-S-0.7	275	40	Dodecane/b	Cresol	92.1	92.9	Number: Co/Mo mole ratio	93
Co-Mo-S-0.1	275	40	Hexadecane/b	Cresol	66.3	97.5	Number: Co/Mo mole ratio	89
Co-Mo-S-0.5	275	40	Hexadecane/b	Cresol	76.4	96.5	Number: Co/Mo mole ratio	89
Co-Mo-S	300	40	-/c	Guaiacol		~84	selectivity is in the O-free products	94
Co-Mo-S/ZrO ₂	300	40	-/c	Guaiacol		~72		95
Co-Mo-S/Al ₂ O ₃	340	40	Dodecane/b	Cresol	~24	~85	-	80
Co-Mo-S/Al ₂ O ₃	250	15	Xylene/c	Phenol	36.4	92.9	-	96
Co-Mo-S/Al ₂ O ₃	300	15	Xylene/c	Phenol	71.9	86.4	-	96
Ni-S	300	40	Dodecane	Cresol	6.8	87.1	-	97
Mo-S	300	40	Dodecane	Cresol	43.1	83.8	-	97
Ni-S+Mo-S	300	40	Dodecane	Cresol	59.2	84.6	-	97
Ni-Mo-S	300	30	Decalin/b	Cresol	77.5	75.4	-	98
Ni-Mo-W-S	300	30	Decalin/b	Cresol	97.8	87.2	-	98
Ni-W-S	300	30	Decalin/b	Cresol	31.1	89.2	-	98
Mo-W-S	300	30	Decalin/b	Cresol	50	89	-	99
Ni-Mo-W-S	300	30	Decalin/b	Cresol	100	94.4	-	99

^a b: batch reactor; c: continuous flow reactor.

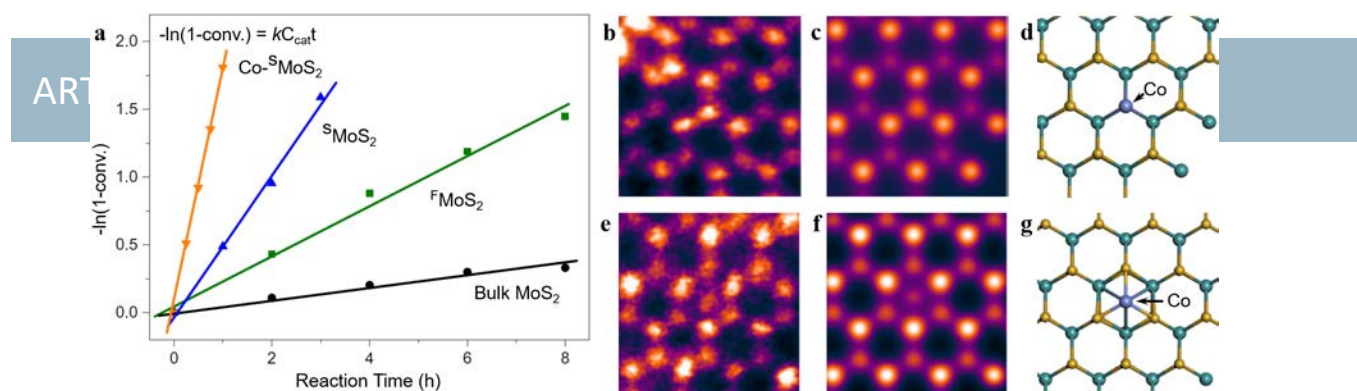


Figure 9. a, Kinetic studies at 3 MPa and 300 °C for HDO of 4-methylphenol to toluene showing activity order of $\text{Co-SMoS}_2 > \text{S-MoS}_2 > \text{F-MoS}_2 > \text{bulk MoS}_2$; b,e, STEM-HAADF image of a Co-substituted S sites in Co-SMoS_2 . c,d,f,g, Image simulation (c,f) and atomic model (d,g) from geometry optimized DFT of a Co-substituted S sites in Co-SMoS_2 . Adapted by permission from Springer Nature, Nature Chemistry, Liu et al.⁴⁰ Copyright (2017).

In order to achieve higher activity and selectivity of sulfide catalysts in HDO, the effect of promoters has also been extensively studied on the Mo-based sulfide catalysts. Shabtai et al.¹⁰⁰ screened the promoters by comparing the rate constants for C-O bond hydrogenolysis of diphenyl ether versus that for hydrogenation of aromatic ring (i.e., hydrogenation of naphthalene). The enhancement of C-O bond hydrogenolysis was found to follow the order of $\text{Ru} > \text{Co} > \text{Cr} > \text{Ir} > \text{Re} > \text{Pd} > \text{Fe} > \text{Rh} > \text{Pt} > \text{Ni}$. It was also found that, besides the nature of the promoter, the concentration of promoter, method of preparation, and sulfiding conditions can influence the selectivity. Given Co is able to form Co-Mo-S active phase, also balancing the cost and activity enhancement of additives, cobalt was usually chosen as promoter on the MoS_2 catalyst in HDO. Recently, Liu et al.⁴⁰ reported a catalyst with isolated Co atoms being covalently bonded to sulfur vacancies of the MoS_2 monolayer sheets for the HDO of cresol. The added Co was found to benefit the formation of new basal S vacancies at Co-S-Mo interfacial sites. Consequently, the Co-SMoS_2 displayed superior activity and selectivity (99.2%) than the non-promoted conventional catalysts as shown in Figure 9. The unique structure led to sufficiently high activity at temperatures as low as 180 °C at 30 bar pressure under which S leaching and deactivation were inhibited. Song et al.⁹¹ employed the self-induced method to regulate the Co-substituted S site to minimize the CoS_x phase and form highly dispersed Co-Mo-S phase. The characterization showed that most of Co-Mo-S phase was on the surface of bulk MoS_2 so that this catalyst displayed high arene selectivity (>85%) and stability in the conversion of a variety of phenolics. Yooksuk et al.⁹² investigated the influence of crystallinity on the catalytic performances by comparing MoS_2 with different morphologies. Under the tested conditions, namely 350 °C and 28 bar, amorphous MoS_2 (surface area: 368 m^2/g) showed much higher apparent activity and arene selectivity (65.6% selectivity at 71.0% conversion) than crystalline one (surface area: 11 m^2/g , 20.3% selectivity at 30.0% conversion) in a 1-h reaction. This was attributed to the smaller particle size and more highly bent sites leading to more S vacancies, which contributed to DDO

selectivity and activity. In addition, incorporation of Co facilitated the formation of S vacancies, which enhanced activity and arene selectivity (above 75%). The promotion from Co was also studied by Wang et al.⁹³ and it was found that adding Co into the MoS_2 decreases the surface area but increases the HDO activity and promotes arene selectivity up to 93.5% at 275 °C and 40 bar. The correlation was made between the number of layers in stack and arene selectivity by adjusting the Co amount in catalysts, suggesting that a higher number of stacking layers enhanced the arene selectivity as explained by the “Rim-Edge” model. The same group also synthesized flower-like Co-Mo-S by adjusting the Co/Mo ratio to 0.3. This specific structure enhanced mass transfer and enlarged edge interfaces. The formed CoS_2 species benefited the η_1 adsorption via oxygen atom, leading to the DDO pathway. In HDO of cresol, DDO route dominated, leading to up to 97.5% arene selectivity at 85.6% conversion⁸⁹. Bui et al.⁹⁴ studied the effect of Co on MoS_2 in HDO of guaiacol. The DDO pathway was significantly facilitated in the presence of CoMoS phase (Co promoter located at the edges of MoS_2 layers) comparing with non-promoted MoS_2 , leading to the promotion of arene selectivity from around 30% to around 83% in the O-free products at 300 °C and 40 bar. These researchers further studied the support (Al_2O_3 , TiO_2 , ZrO_2) effect for CoMoS catalysts, showing that $\text{CoMoS}/\text{ZrO}_2$ displayed high selectivity towards $\text{C}_{\text{aromatic-O}}$ hydrogenolysis (72% in the O-free products) with demethoxylation and DDO as the main reaction pathways⁹⁵. This was attributed to the surface hydroxyl groups on ZrO_2 that might have influenced the adsorption configuration. In contrast, CoMoS with Al_2O_3 and TiO_2 as supports catalyzed the demethylation, forming catechol followed by both DDO and HYD.

Ni is another promoter in the sulfide catalysts with the main role of increasing the activity although the arene selectivity is usually negatively impacted¹⁰¹⁻¹⁰³. Bunch et al.^{104, 105} studied the reaction network in HDO of benzofuran over sulfided Ni-Mo/ Al_2O_3 catalyst. In the sulfide form, Ni addition maintained the hydrogenolysis as dominant reaction pathway, but the

produced ethylbenzene was readily hydrogenated to ethylcyclohexane. It should be noted that co-feeding H_2S promoted the conversion of 2,3-dihydrobenzofuran but inhibited the conversion of 2-ethylphenol (EP), which should not occur if the reaction took place via direct C-O bond cleavage. This led to the proposition of another reaction pathway: partial hydrogenation of the ring followed by dehydration to form arene. It was also proposed that the S vacancies acted as the ring-hydrogenation sites^{104, 105}, which is contradictory to the widely accepted conclusion that the S vacancies contribute to the direct C-O bond cleavage. Wang et al.⁹⁰ investigated the Ni-Mo sulfide catalyst in HDO of cresol and showed that incorporation of Ni could promote the activity. With the increase of Ni content, however, the toluene selectivity gradually decreased. In comparison, they also synthesized NiS_x with microwave-assisted hydrothermal method and mixed it with MoS_2 to promote the activity of HDO of cresol⁹⁷ at 300 °C and 40 bar. It was found that mixing NiS_x with MoS_2 enhanced the conversion but had no effect on the product distribution. The comparison of Ni-Mo-S (Ni atom on the edges of MoS_2 layers) with NiS_x/MoS_2 (MoS_2 supporting NiS_x) and physically mixed NiS_x+MoS_2 implied that synergies between NiS_x and MoS_2 , other than forming Ni-Mo-S phase, contributed to the promotion in activity⁹⁰. Therefore, the remote control model^{90, 106} was proposed to interpret the results that cresol mainly adsorbs on MoS_2 site and reacts with active H dissociated on NiS_x and transferred to MoS_2 .

While WS_2 is a typical hydrotreating catalyst, it can also be incorporated into Mo-based sulfide to achieve higher reactivity. Prior to the HDO reaction, the improvement in activity by incorporating W to sulfide catalysts was also reported in the HDS reactions^{107, 108}. The amount of W incorporated can adjust the number of active sites (proposed as the S vacancies), leading to a typical “volcano” curve relationship between activity and W content¹⁰⁷. With this inspiration, besides Co and Ni, W was also used as a promoter in HDO on the metal sulfide catalysts. The Ni-Mo-W sulfide synthesized with mechanical activation method was also reported to exhibit arene selectivity above 95% in HDO of cresol at 300 °C and 40 bar^{98, 99}. W was proposed to promote the DDO pathway by increasing the Ni atoms engaged in the mixed “NiMo(W)S” active phase. However, when the synthesis method was changed to hydrothermal method using different precursors as reported by Wang et al.¹⁰⁹, the slab length was drastically decreased from ~100 nm (mechanical activation synthesis⁹⁸) to < 20 nm, leading to increased number of corner sites for HYD pathway. As a result, arene selectivity was decreased to around 30% whereas the reactivity was enhanced by increased number of active sites via W addition.

Since the sulfide catalysts have been shown promising in the selective HDO of phenols, and the current petroleum refinery system also employs sulfide catalyst for hydrotreating, from practical application point of view, co-processing of aromatic oxygenates and fossil fuels is considered as a potentially economic approach to selectively produce arenes being blended with traditional fuel. One benefit from co-processing is to reduce the cost since it utilizes the existing infrastructure and distribution systems, and avoids the risk of establishing a new parallel system for bio-oil¹¹⁰. In a co-processing study conducted by Pinheiro et al.¹¹¹, the aromatic oxygenates (3.38 wt.% for

anisole, 1.94 wt.% for guaiacol) did not show inhibition to HDS and HDN of straight-run gas oil (SRGO). Bui et al.¹¹⁰ studied co-processing guaiacol (5000 ppm) as a model compound with SRGO using Co-Mo-S on alumina in HDS process. Partial deoxygenation products (i.e. phenol, methylphenol etc.) dominated with limited ring saturation at 300 °C and 40 bar H_2 .

An issue for the application of sulfides is deactivation that could be caused by the oxygen-containing molecules, including the oxygenate reactant and water which is ubiquitous in the feedstock and also the product in HDO process. It was found that Mo has much higher affinity for oxygen than sulfur, which can lead to the replacement of sulfur by oxygen to form oxides (which is less active than sulfides)^{112, 113} and ultimately, the catalyst deactivation¹¹⁴. Co-feeding sulfide additive was used to maintain the sulfide form and reactivity of catalysts¹¹⁵. Gutierrez et al.¹¹⁶ studied the HDO of guaiacol using sulfided Co-Mo and Ni-Mo catalysts. It was found that the methoxy group in guaiacol is able to react with the SH^- to form the S-containing compounds in the products (whereas phenol hardly causes the S-leaching). Overall, although sulfides may lead to high arene selectivity, conventional hydrotreating catalysts³³ suffer from the issues like sulfur contamination in products, accumulated coking and deactivation due to the loss of sulfur^{11, 117}, which are the major barriers for the further application in HDO⁷⁷. Efforts have been made on the development of alternative sulfur-free catalysts including base metal catalysts, noble-metal-based catalysts, and metal carbides, nitrides, phosphides, etc.³².

4.2 Base metals (oxides)

Base metals are generally oxophilic, inexpensive and environmentally benign, making them as promising candidates for selective HDO catalysts. Among the base metal catalysts, Fe, Ni and Mo have been extensively studied for HDO of phenols. Although both experimental studies and theoretical calculations have demonstrated that planar adsorption, a configuration facilitating aromatic ring saturation, is the most

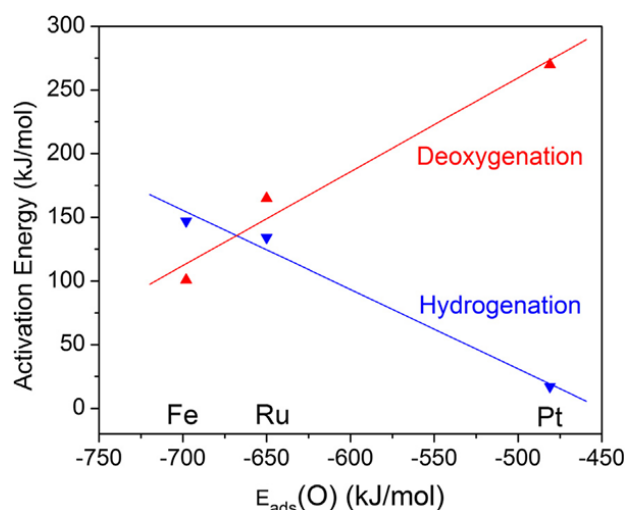


Figure 10. Correlation between the intrinsic energy barrier for the hydrogenation reaction and deoxygenation reaction of phenoxy on different metal surfaces and the adsorption energies of the atomic oxygen (oxophilicity) on these metal surfaces. Reprinted from Tan et al.¹²¹ Copyright (2017), with permission from Elsevier.

favorable adsorption configuration for phenol over Fe and Ni¹¹⁸⁻¹²⁰, high arene selectivity can still be obtained by controlling key parameters such as the intrinsic oxophilicity, particle size, and oxygen vacancies, etc. as proposed below.

4.2.1 Key factors affecting the arene selectivity on base metal (oxide) catalysts

Oxophilicity describes the tendency to form oxide so that it is related to the reactivity in abstracting the O in phenols. By combined experimental and theoretical studies, Tan et al.¹²¹ investigated the HDO of anisole over Fe and noble metals (Pt and Ru). The intrinsic energy barriers for the hydrogenation reaction and deoxygenation reaction of phenoxy are correlated to oxophilicity expressed as adsorption energies of the atomic oxygen, i.e. with the increase of oxophilicity, energy barrier for the direct C-O bond cleavage decreases while barrier for hydrogenation increases, as shown in Figure 10. Although Fe(110) has the same planar adsorption configuration for anisole as noble metals such as Pt(111) and Ru(0001), the higher oxophilicity of Fe leads to the lower activation barrier for direct cleavage of C-O bond and high arene selectivity. In another study, the oxophilic Fe has been calculated to interact preferably with oxygen-containing functional groups, distorting the C-O bonds to a greater degree, which should facilitate the direct C-O bond cleavage and formation of arenes¹¹⁹.

Oxygen vacancies, similar to the sulfur vacancies on sulfide catalysts, are proposed to activate the C-O bond and contribute

4.2.2 Selective base metal (oxide) catalysts

Table 3. Performances of base metal (oxide) catalysts with high arene selectivity in the HDO of aromatic oxygenates.

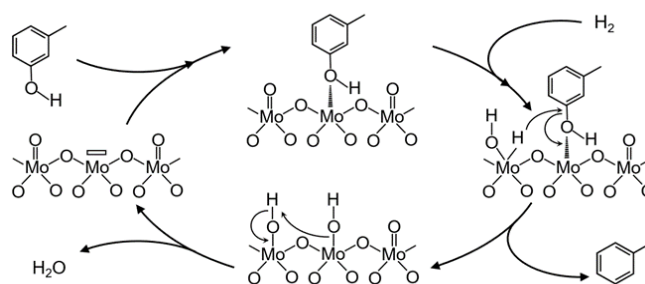


Figure 11. Mechanism of the direct deoxygenation (DDO) route of m-cresol on the vacancies of molybdenum oxide site species.³³

to the improved arene selectivity over metal oxide¹²². Gonçalves et al.³³ correlated the number of oxygen vacancies of MoO_x on different supports measured by oxygen chemisorption with DDO reaction rates. The correlation suggests that the oxygen vacancies involving reduced Mo species (Mo⁵⁺ and Mo⁴⁺) play a major role in the DDO reaction route, as shown in a proposed reaction mechanism in Figure 11. Briefly, the oxygen vacancies, i.e. coordinately unsaturated sites (CUS) of Mo, created by H₂ reduction interact with O in the phenols and weaken the C-O bond⁵⁷ which is further cleaved by the hydride species originated from H₂ dissociation. The vacancies are subsequently recovered by releasing water to complete the catalytic cycle. The function of oxygen vacancies is similar to the oxophilicity model proposed for the metallic base metal such as Fe^{123, 124}, i.e. C-O bond scission is due to the strong interaction between hydroxyl and metallic surface, followed by elimination of aryl and hydroxyl groups with dissociated H to form arene and water.

Catalyst	Reaction condition			Substrate	Conv. (%)	S _{arene} (%)	Ref
	T(°C)	P (bar)	Solvent/Reactor ^a				
Fe	300	1	-/c	Cresol	1 ~ 10	>90	125
Fe	300	1	-/c	Cresol	21	90	124
Fe/SiO ₂	400	1	-/c	Guaiacol	>80	>90	126
Fe/SiO ₂	375	1	-/c	Anisole	8	85	121
Fe/SiO ₂	300	1	-/c	Cresol	8.8	60.2	64
Co/SBA-15	300	1	-/c	Anisole	62	70	127
Ni/CeO ₂	290	3	-/c	Anisole	96	58	56
Ni/TiO ₂	290	3	-/c	Anisole	51	74	56
5wt%Ni/SiO ₂ -2nm	300	1	-/c	Cresol	95.6	79.2	128
5wt%Ni/SiO ₂ -5nm	300	1	-/c	Cresol	93.6	68.7	128
5wt%Ni/SiO ₂ -10nm	300	1	-/c	Cresol	98.9	68.1	128
Ni/SiO ₂	300	1	Methanol/c	Phenol	>90	>90	129
Ni-based	450	7.9	-/c	Guaiacol	100	~85	130
Ni/Al ₂ O ₃	260	1	-/c	Cresol	30	67.8	131
Ni-Fe/SiO ₂	300	1	-/c	Cresol	13.7	52.6	64
Ni/Ce _{0.3} Nb _{0.7} O ₂	300	1	-/c	Phenol	9.53	86.9	132
Ni/Nb ₂ O ₅	300	1	-/c	Phenol	10.1	90	132
MoO ₃	325	1	-/c	Cresol	48.9	99.4	57
MoO ₃	300	5	Octane/b	Phenol	23.1	73.9	133
MoO ₃ /ZrO ₂	320	1	-/c	Cresol	78	99	122
MoO ₃ /TiO ₂	320	1	-/c	Cresol	47	99	122
MoO ₃ /CeO ₂	320	1	-/c	Cresol	8	97	122
MoO ₃ /Al ₂ O ₃	320	1	-/c	Cresol	13	76	122
MoO ₃ /SiO ₂	320	1	-/c	Cresol	10	90	122
MoO ₃	320	1	-/c	Cresol	13	99	122
MoO _x /SiO ₂	340	40	-/c	Cresol	23.8	81.9	33
MoO _x /SBA-15	340	40	-/c	Cresol	23.9	82.8	33
MoO _x /Al ₂ O ₃	340	40	-/c	Cresol	22.1	85.5	33
MoO ₃	325	41	Decalin/b	Cresol	61	63	87
MoO ₃ /TiO ₂	350	25	-/c	Phenol	~28	~89	134
Ni-Mo/SiO ₂	410	1	-/c	Phenol	99	99	135

^a b: batch reactor; c: continuous flow reactor.

Table 3 summarizes the representative base metal (oxide) catalysts with high arene selectivity in HDO of aromatic oxygenates. Fe-based catalysts have been studied for the phenolic HDO recently which show high arene selectivity in the vapor-phase reactions. Olcese et al.^{37, 126, 136} studied Fe supported on SiO₂ and active carbon (AC) catalysts. Both guaiacol model compound and the real lignin pyrolysis vapor products were used as reactants, and hydrogenation of aromatic ring was barely observed. Using guaiacol substrate, an arene yield of 38%, along with other aromatic oxygenates products (i.e., phenol, anisole, cresol), was achieved at 74% conversion over Fe/SiO₂ under the conditions studied (400 °C, 1 bar)³⁷. α -Fe was identified as the major phase after reaction, suggesting the metallic Fe are the active sites. Moreover, due to its weak acidic nature, SiO₂ support exhibited the mitigated coke formation during HDO, leading to enhanced catalyst

stability. With the simulated lignin pyrolysis vapor mixture (i.e., guaiacol + H₂ + CO + CO₂ + H₂O), the initial arene selectivity of Fe/SiO₂ was higher than 90% at conversion above 80%¹²⁶. TEM of deactivated catalyst showed coke formation in the vicinity region of iron particles on SiO₂. In contrast, Fe/AC produced phenol and catechol as the main products with arene selectivity < 2%. These results seemingly indicate the Fe-SiO₂ interface is the HDO active site. However, recent studies on Fe/AC¹²³ and the support-free Fe¹²⁴ displayed high reactivity for arene production in the HDO of phenolics (i.e., guaiacol and cresol) at 450 and 300 °C, respectively. Together with their DFT studies¹²⁰, a direct C-O bond cleavage was proposed as the most energetically and kinetically favorable pathway in comparison with others parallel ones like tautomerization, followed by partial hydrogenation and dehydration. These results suggest that Fe itself could serve as the active sites in the selective HDO of phenolics to produce arenes. In the conversion of real

pyrolysis vapor, the Fe/SiO₂ could reduce O content by producing benzene and phenol from molecules containing two or more oxygen atoms per aromatic ring (i.e. guaiacol, catechol and vanillin)¹³⁶. The catalytic performance of Fe was also studied experimentally and theoretically using anisole as a reactant¹²¹. The results indicated that the strong metal oxophilicity facilitated the direct scission of C_{aromatic}-O bond of the surface phenoxy to benzene, rather than that of C_{sp³}-O bond (demethylation) to phenol followed by a secondary reaction (dehydroxylation). These studies imply that Fe-based catalysts are potentially selective, though it suffers low activity/stability. To improve the activity/stability of Fe, promoters such as noble metals¹²³ (will be detailed in section 4.3.3) and Ni have been demonstrated to be efficient. Nie et al.⁶⁴ employed Ni and prepared the bimetallic Fe-Ni on SiO₂ for cresol HDO at 300 °C and 1 bar. While the monometallic Ni mainly saturated the aromatic ring, the bimetallic catalysts exhibited comparable arene selectivity (> 90%) but much higher activity than the monometallic Fe. Tautomerization to methylcyclohexadienone followed by a carbonyl hydrogenation and dehydration was proposed as the main reaction pathway. When the oxophilic Fe is alloyed with Ni, its interaction with the aromatic ring is weakened but that with carbonyl group is enhanced. Their DFT calculations also showed a repulsion to the aromatic ring from Ni-Fe alloy surface. These factors contributed to the promoted arene selectivity. It is worth mentioning that, other than the unique properties of catalysts, the arene selectivity could also be significantly influenced by the reacting conditions that determine the thermodynamic equilibrium. For example, on the same Ni-Fe catalysts, another study shows much lower (~ 10%) arene selectivity at 250 °C and 10 bar (versus the >90% arene selectivity at 300 °C and 10 bar)¹³⁷.

Ni-based catalysts are another group of catalysts being widely investigated in HDO. Monometallic Ni was supported on different supports like γ -Al₂O₃, carbon, TiO₂, CeO₂, SBA-15, Al-SBA-15 for the HDO of anisole at around 300 °C⁵⁶. The results suggested that the nature of supports was an important factor in influencing the product distribution, e.g. strong metal-

support interaction reduces the hydrogenation capacity. For example, the Ni/TiO₂ with strong metal-support interaction displayed the highest arene selectivity (~80%) among the catalysts studied. Yang et al.¹²⁸ synthesized 5%Ni/SiO₂ with different preparation methods to adjust the particle sizes from 2 nm to 22 nm. As the Ni particle size decreased, both the intrinsic reaction rates (TOF) of cresol conversion and arene formation increased with the latter increasing more dramatically. As a result, both arene selectivity and activity were improved (Figure 12). The size effect was ascribed to the increased number of highly coordinatively unsaturated surface Ni sites on smaller particles on which the barrier for DDO pathway was lowered by a facilitated adsorption and stabilization of -OH in the transition state, evidenced by the DFT calculations. In another study on Ni/SiO₂ for HDO of phenol, it was found that the activity toward DDO was enhanced as Ni particle size increased from 1.4 nm to 3.7 nm, leading to increased arene selectivity from 16% to 99%¹²⁹. This result suggests that there could be a volcanic dependence of selectivity on the Ni particle size with 2-3.7 nm being the most selective ones. Other Ni-based catalysts such as Ni/Al₂O₃ and Ni for commercial hydroprocessing have also been investigated showing high arene selectivity in vapor-phase reaction^{130, 131}. Resende et al.¹³² supported Ni on CeNb_xO_y for HDO of phenol at 300 °C and 1 bar. Tautomerization followed by carbonyl hydrogenation and dehydration was proposed as the main reaction pathway to produce benzene. It was observed that a higher Nb content led to enhanced arene selectivity and suppressed ring saturation, which was attributed to the highly oxophilic nature of Nb species that benefited the formation of oxygen vacancies. The oxygen vacancy sites strongly interacted with O in phenol, and thus hydrogenation of carbonyl group was enhanced to produce benzene.

Mo-based catalysts, such as oxide, sulfide, carbide, nitride, and phosphide, are commonly selective to DDO of phenolics. By comparing these Mo based catalysts, Whiffen et al.⁸⁷ found that lowering the electron density of the Mo led to a higher reactivity. In addition, the presence of Brønsted acid sites and

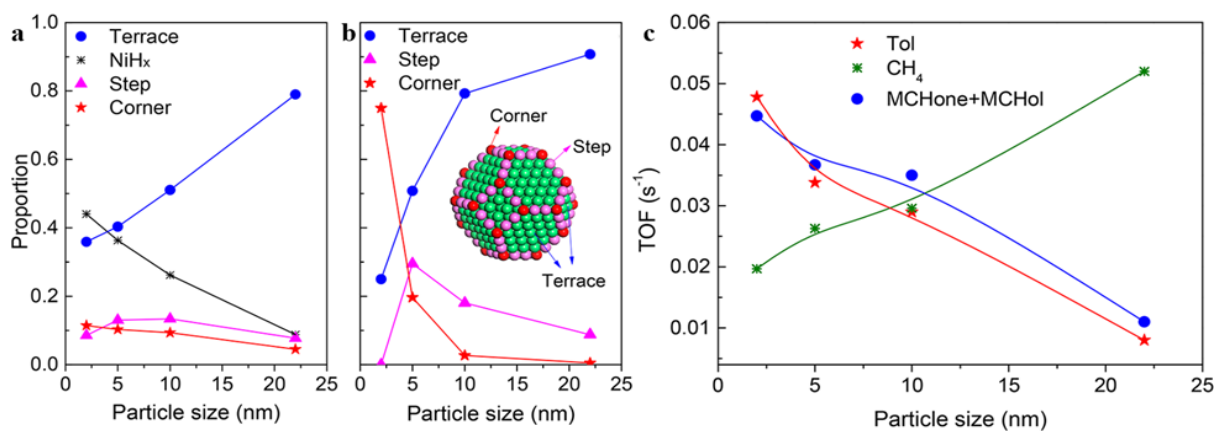


Figure 12. a, Proportion of different surface sites obtained from H₂-TPD, b, theoretical proportion based on a model of cube-octahedron which is shown in the inset picture as a function of Ni particle size and c, turnover frequencies of m-cresol conversion to different products at reaction conditions: T = 300 °C, P = 1 atm, TOS = 30 min. Adapted with permission from Yang et al.¹²⁸ Copyright (2018) American Chemical Society.

anionic vacancies were also proposed to promote the activity of partially reduced MoO_x in the HDO of cresol. Prasomsri et al.⁵⁷ investigated the MoO_3 for the vapor phase HDO of a group of phenolics at 325 °C and 1 bar. For all the aromatic compounds studied, MoO_3 tended to cleave the $\text{C}_{\text{aromatic}}\text{-O}$ bonds over the weaker $\text{C}_{\text{aliphatic}}\text{-O}$ bonds. The induction period for fresh catalysts could be eliminated by a 3-hour pre-reduction, and the oxycarbohydride ($\text{MoO}_x\text{C}_y\text{H}_z$) phase could be readily formed after the introduction of carbon source (i.e. cresol). Therefore, the Mo^{5+} Lewis acid center (i.e. oxygen vacancy) was proposed as active site for the enhanced $\text{C}_{\text{aromatic}}\text{-O}$ bond cleavage. The same group also studied the MoO_3 supported on different oxides (i.e., SiO_2 , Al_2O_3 , TiO_2 , ZrO_2 and CeO_2) for vapor-phase HDO of cresol at 320 °C and 1 bar¹²². All the catalysts displayed high arene selectivity with no ring saturation. It was found that the supports led to different proportions of Mo^{5+} species correlated with the reactivity and stability. For the catalysts showing low reactivity, the Mo species were dominated with Mo^{6+} , Mo^{4+} or metallic oxidation state. The results suggest the coordinatively unsaturated Mo^{5+} sites involved in the DDO reaction, as demonstrated by the oxygen-vacancy driven mechanism. Recently, operando near-ambient pressure (NAP) XPS was also employed to study the active site and reaction mechanism on the MoO_3 ¹³⁸. Mo species was found to transit between 5+ and 6+ oxidation state during reaction conditions, which provided a solid evidence for the proposed oxygen-vacancy driven mechanism. The bimetallic system Ni-Mo was studied in the HDO of anisole, phenol and guaiacol, achieving ~98% arene selectivity at 410 °C¹³⁵. Arene selectivity maintained for only about 1.5 h before the deactivation occurred. However, combustion in air flow at 550 °C was able to regenerate the catalyst, which showed practically stable performance in the 14 regeneration cycles tested. Based on this observation and the NH_3 -TPD results showing the decreased NH_3 adsorption on spent catalyst compared with fresh one, carbon deposition was hypothesized to cover the active sites and change the Mo oxidation state, leading to the deactivation of catalysts in terms of both activity and selectivity.

Yang et al.¹²⁷ compared Ni and Co supported on SBA-15 in vapor-phase HDO of anisole 300 °C and 1 bar. Although Co/SBA-15 displayed lower reactivity than Ni/SBA-15, the arene

selectivity was much higher, reaching to around 70% at high conversion. In the study using bimetallic Ni-Fe⁶⁴, the performances of monometallic Ni and Fe were also compared. The arene selectivity of Fe (60.2%) was much higher than that of Ni (14.2%), while Mo oxide displayed higher arene selectivity than Fe, by cross-comparison of literature reports^{62, 87}. The performances of these base metals could be correlated with their intrinsic oxophilicities that is discussed in section 5.

4.3 Noble-metal-based catalysts

For clarification, “noble-metal-based catalyst” in the review are mainly divided into two groups, i.e., catalysts with solely noble metal functionality (i.e., monometallic noble metal supported on an inert support) and catalysts bearing not only noble metal but other functionalities that may play synergistic role with the noble metal in HDO reactions.

4.3.1 Performances of monometallic noble metal catalysts

Over noble metals, planar configuration is the most favorable adsorption for phenols, as has been confirmed by both experimental results and theoretical calculations¹³⁹⁻¹⁴¹. This adsorption configuration, together with the facile activation of H_2 , leads to the dominant hydrogenation of aromatic ring on noble metals in HDO of phenolics, especially under high hydrogen pressure^{55, 142, 143}. Therefore, the monometallic noble metals usually display low arene selectivity. Carbon is typically used as a support to minimize the support effect¹²³ in the HDO of phenols. A summary of catalytic performances of carbon supported noble metal catalysts are shown in Table 4. In general, noble metals (Ru, Rh, Pd, Pt et al.) predominantly produce ring-saturated products. The underlying reasons for ring-saturation have been extensively discussed in the previously reported reviews^{18, 32, 144, 145}. However, it should be noted that several exceptions can be found on the monometallic noble metals. For example, Pd/C¹²⁴ and Pt/C¹⁴⁶ were recently reported showing higher arene selectivity (Table 4, entry 7 and 9). A further looking into the cases indicate that, over the same Pt/C catalyst¹⁴⁶, distinct arene selectivity was reported under different reaction conditions, i.e. 47% at 350 °C and 5 bar versus 0% at 250 °C and 20 bar (Table 4, entry 9 vs entry 10). This could result from the controls by both kinetics and thermodynamic equilibrium (Figure 5).

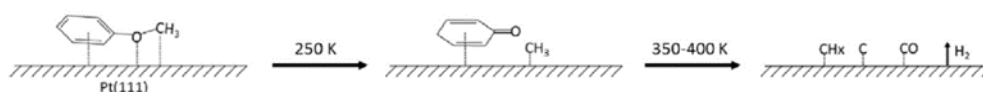
Table 4. Catalytic performances of monometallic noble metals.

Entry	Catalyst	Reaction condition			Substrate	Conv. (%)	S_{arene} (%)	Ref
		T(°C)	P (bar)	Solvent/Reactor ^a				
1	Ru/C	275	50	Hexadecane	Propylphenol	100	0	143
2	Ru/C	275	50	Hexadecane	Eugenol	100	0	143
3	Ru/C	200	50	Water/b	Phenol	100	0	147
4	Rh/C	200	50	Water/b	Phenol	100	0	147
5	Pd/C	200	50	Water/b	Phenol	100	0	147
6	Pd/C	250	50	Water/b	Phenols	100	0	148
7	Pd/C	300	1	-/c	Cresol	10	78	124
8	Pd/C	275	100	-/b	Phenol	100	0	149

9	Pt/C	350	5	-/c	Cresol	32-38	47	146
10	Pt/C	250	20	-/c	Cresol	32-38	0	146
11	Pt/C	200	50	Water/b	Phenol	100	0	147

^a b: batch reactor; c: continuous flow reactor.

Anisole on Pt(111) surface



Anisole on 0.2 ML Zn/Pt(111) surface

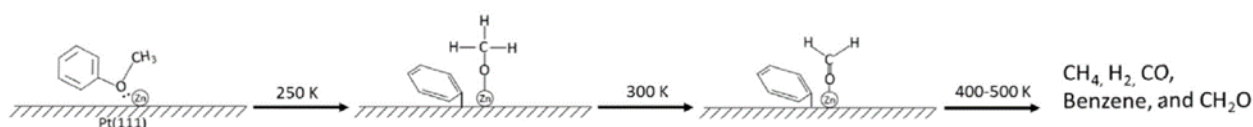


Figure 13. Proposed pathways and intermediates for the adsorption and reaction of anisole on Pt(111) and Zn/Pt(111) surfaces. Reprinted from Shi et al.¹⁵¹ Copyright (2016), with permission from Elsevier.

4.3.2 Approaches to control the arene selectivity: noble metal with added new functionalities

In contrast to the monometallic noble metal catalysts, bimetallic catalysts containing noble and base metals/metal oxides have been demonstrated to be highly efficient for selective HDO to produce arenes from phenolics. In this particular case, the highly selective DDO of the bimetallic catalysts is mainly ascribed to the adjusted adsorption geometry of phenols or newly gained functionalities/properties (e.g., oxophilicity). As proposed and demonstrated on the sulfide catalysts⁷⁸, a perpendicular adsorption configuration of phenols enhances the direct cleavage of C-O bond and thus inhibits the hydrogenation of aromatic ring. A similar effect is also proposed for the noble metals, such as supported Pt-based¹⁵⁰ and Ru-based catalysts¹¹⁷. Since the noble metals favor planar configuration, the function of metal additive is proposed to tilt away the aromatic ring from surface. Shi et al.¹⁵¹ studied the function of Zn to Pt catalyst using HDO of anisole as a model reaction. Over monometallic Pt(111), the strong interaction between phenyl ring and the surface, which facilitated the ring saturation, was observed using temperature programmed desorption (TPD) and electron energy loss spectroscopy (EELS). However, over the Zn-modified Pt(111), anisole was found to bond to surface by oxygen at Zn or adjacent Pt sites with ring tilted away from the surface as shown in Figure 13. This change in adsorption geometry led to the significant difference in catalytic performance: Pt/C catalyst converted anisole to saturated products with 100% selectivity while around 70% of products was phenol from CH₃-O bond cleavage over PtZn/C catalyst.

Another way to promote the arene selectivity is via additives/supports with high oxophilicity. This approach has been extensively studied and a detailed discussion is shown in the next section. A brief example is the comparative study on Ru-based catalysts with different supports¹⁵², showing Ru/TiO₂ had high selectivity toward DDO pathway and arene production. H₂ spillover over small Ru particles was found to generate the Ti³⁺ sites, and the dominant benzene produced over Ru/TiO₂

was attributed to the oxophilic Ti³⁺ sites which interacted strongly with oxygen in phenol, weakening the C-O bond and facilitating the direct bond cleavage as shown in Figure 14.

DDO at reduced metal-interface sites

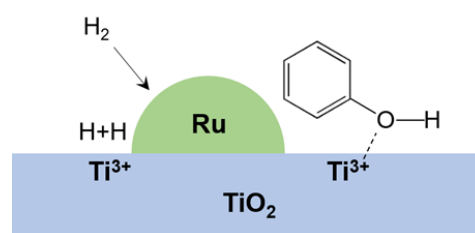


Figure 14. Schematic illustration of DDO reaction over Ru particle on TiO₂: Ru dissociates hydrogen reducing TiO₂ to Ti₄O₇ or other Ti³⁺ defect sites where the phenol hydroxyl group can form a Ti-O bond, leading to hydrogenolysis in a DDO mechanism.¹⁵²

4.3.3 Selective noble-metal-based catalysts

Among the selective noble-metal-based catalysts (Table 5), Ru has lower barrier for direct dehydroxylation than other noble metals such as Rh, Pd, Pt¹⁵³. However, besides the dehydroxylation¹⁵⁴, Ru is also highly active in activating H₂ for hydrogenation and cracking the reactants/intermediates to methane^{121, 153}. A base metal (oxide) is necessary to gain new functionality and modification for the Ru-based catalysts. Recently, Shao et al.¹⁵⁵ reported Ru/Nb₂O₅ catalyst for direct HDO of organosolv lignin showing 64 wt.% arene selectivity and a total mass yield of 35.5 wt.% in 20h reaction, both of which were much higher than that of Ru supported on ZrO₂, Al₂O₃ and TiO₂. This catalyst for HDO of cresol displayed 80% arene selectivity at 250 °C and 5 bar H₂. A combined inelastic neutron scattering (INS) and DFT calculation confirmed the different binding between adsorbed phenol and surface/reaction activity over different supports. Nb₂O₅ strongly adsorbed phenol and

significantly reduced the energy barrier for $C_{\text{aromatic}}\text{-O}$ bond cleavage as shown in Figure 15 while Ru contributed to dissociation/activation of H_2 . In addition, the generated arene desorbed readily which further mitigated the hydrogenation of the aromatic ring. All these factors jointly led to this high arene selectivity. Besides Nb_2O_5 , Ru could also be modified with WO_x which was developed by Huang et al.¹⁵⁶ on the Ru- WO_x bifunctional catalyst. Based on the activity results using possible intermediates, direct C-O bond cleavage which involved O atom in adsorbed phenol being chelated with oxophilic sites (Lewis sites from W and supports) was proposed as the likely mechanism. The synergy between Ru (activating H_2) and W (activating C-O bond) provided this catalyst with high selectivity in cleaving $C_{\text{aromatic}}\text{-O}$ bond in phenols and lignin-derived ethers. By adjusting the ratio of Ru/W and selecting an appropriate support, Ru- WO_x catalyst achieved 81% arene selectivity in HDO of butylphenol at 270 °C and 20 bar H_2 .

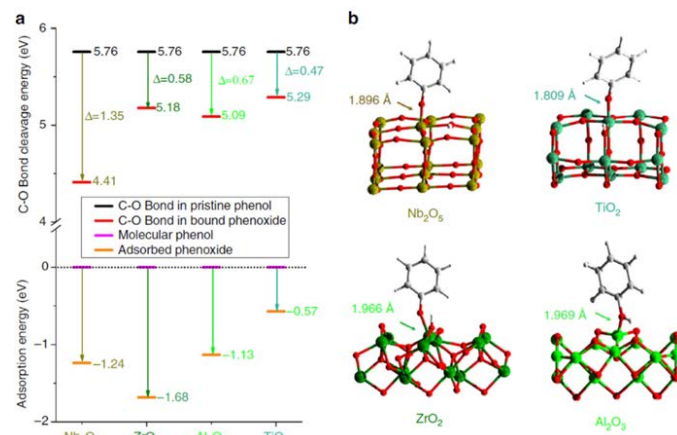


Figure 15. a, Calculated energies for phenol adsorption and disassociation of the C-O bonds upon adsorption over Nb_2O_5 , ZrO_2 , Al_2O_3 and TiO_2 . b, Views of the corresponding DFT-optimized structural models for the phenoxide. Reprinted from Shao et al.¹⁵⁵

Table 5. Performances of noble-metal-based catalysts with high arene selectivity in the HDO of aromatic oxygenates or lignin.

Catalyst	Reaction condition			Substrate	Conv. (%)	S_{arene} (%)	Ref
	T(°C)	P (bar)	Solvent/Reactor ^a				
Ru/TiO ₂	300	45.8	-/b	Phenol	12	85	152
Ru/TiO ₂	300	45.8	Water as additive/b	Phenol	30	95	157
Ru/Nb ₂ O ₅	250	5	Water/b	Cresol	100	80	155
Ru- WO_x /SiAl	270	20	Water/b	Butylphenol	100	81	156
Ru- WO_x /ZrO ₂	270	20	Water/b	Butylphenol	27	65	156
Ru/HZSM-5	240	2	Water/b	Guaiacol	100	95	36
Ru/HZSM-5	240	2	Water/b	Methyl-guaiacol	100	93	158
Ru/HZSM-5	240	2	Water/b	Syringol	100	94	158
Ru/TiO ₂	300	10	Decane/b	Anisole	81	79	159
RuFe/TiO ₂	300	10	Decane/b	Anisole	98	82	159
Ru-Fe	300	1	-/c	Cresol	76	98	124
Pd/ZrO ₂	300	1	-/c	Phenol	77	66	160
Pd/TiO ₂	300	1	-/c	Phenol	7	66.8	74
Pd/Nb ₂ O ₅	300	1	-/c	Phenol	6.6	80.2	161
Ni@Pd/SiO ₂ -Al ₂ O ₃	450	1	-/c	Guaiacol	96	82	162
Pd/SiO ₂ -Al ₂ O ₃	450	1	-/c	Guaiacol	83	73	162
Pd-Fe/C	450	1	-/c	Guaiacol	100	83	123
Pd-Fe	300	1	-/c	Cresol	1 ~ 6	>90	125
Pd-Fe	300	1	-/c	Cresol	48	92	124
Pt/Hbeta	400	1	-/c	Cresol	100	>90	163
Pt/Hbeta	400	1	-/c	Anisole	100	>90	164
Pt/SiO ₂	400	1	-/c	Anisole	100	69	164
Pt/SiO ₂	400	1	-/c	Cresol	91	>75	163
Pt/Al ₂ O ₃	260	1	-/c	Cresol	30	65	131
Pt/TiO ₂	300	1	-/c	Cresol	17	89	63

monometallic Fe catalyst could be correlated with the gradual oxidation of Fe during HDO of cresol, whereas the Pd-Fe catalyst showed negligible oxidized Fe species and thus no deactivation⁷¹. This correlation supported the proposed role of Fe and Pd in the synergetic catalysis. The Pd on different supports were employed to study the reaction pathway and intermediates for HDO of phenol using a fixed-bed reactor 300 °C and 1 bar¹⁶⁰. Pd on SiO₂ mainly saturated the aromatic ring to produce cyclohexanone, while Pd on the oxophilic support (i.e. ZrO₂) displayed ~67% selectivity towards benzene. The *in situ* DRIFTS measurements suggested the involvement of 2,4-cyclohexadienone as the key intermediate in both pathways producing benzene and ring-saturated products. Over Pd/ZrO₂, the C=O bond in this keto tautomer was hydrogenated to form cyclohexadienol, followed by rapid dehydration to produce benzene. Pd not only activated H₂, but also contributed the Pd-support interface for dehydration (pure support showed negligible dehydration activity). Based on these results, it was proposed that the product distribution in HDO of phenols could be controlled by using supports with varied oxophilicity. These researchers further investigated the effect of support on the reaction mechanism over the Pd catalysts⁷⁴. The DRIFTS spectra showed that phenol adsorbed dissociatively over CUS metal cations, an oxophilic site. The greater interaction between oxygen in the enone intermediate enhanced the selective hydrogenation of C=O bond, consequently promoting the benzene formation in the proposed reaction pathway, as occurred over the Pd/TiO₂ showing 66.8% selectivity to benzene. Similar study by Barrios et al.¹⁶¹ reported the Pd/Nb₂O₅ catalyst for vapor-phase HDO of phenol at ambient pressure. Due to the strong interaction between the Nb cations and the oxygen in reactant as well as the enhanced hydrogen activation by Pd, Pd/Nb₂O₅ converted phenol to benzene with 80.2% selectivity, which was much higher than that of SiO₂ supported Pd catalyst that mainly saturates the aromatic ring. This strong interaction was correlated with the typical band of C=O in DRIFTS, suggesting the Nb⁴⁺/Nb⁵⁺ cations promotes the formation of ketone intermediates during the reaction.

Pt-based catalysts could also be selective to arene by surface modification and adjusting the reaction conditions. Zhu et al.^{163, 164} studied the bifunctional Pt/HBeta catalyst for HDO of cresol at 400°C and 1 bar, leading to arene as the major product (>90%) and methylcyclohexane as the minor one. Pt/HBeta had a turnover frequency that was 3 times higher than that of Pt/SiO₂, which was proposed due to the synergetic bifunctionality: Pt partially hydrogenated the ring to form cyclohexadienols and Brønsted acid site catalyzed the dehydration to produce arene. In addition, Pt significantly reduced the coking on acid sites to mitigate the deactivation. Further study¹⁶⁵ showed this catalyst might favor the adsorption configuration as phenyl ring on Pt and oxygen on acid sites. Brønsted acid sites catalyzed transalkylation and deoxygenation while Pt sites catalyzed the hydrogenolysis of O-CH₃ in anisole and partial hydrogenation of the ring, resulting in the bifunctionality of both transalkylation to mitigate carbon loss and deoxygenation over Pt/HBeta due to the close proximity of Pt and acid sites. Phuong et al.¹³¹ investigated the Pt/Al₂O₃ catalyst in the vapor phase HDO of cresol under 300 °C and 1 bar. The HDO mechanism was proposed as two consecutive steps: partial hydrogenation of the aromatic ring to form cyclic alcohol (e.g. methylcyclohexadienol) followed by dehydration to produce toluene. Since ring hydrogenation was slower than its sequential dehydration, 65% arene selectivity was achieved at 30% conversion. Nie et al.⁶³ studied the kinetics of cresol HDO over supported Pt-based catalysts by employing the Langmuir-Hinshelwood model.

Tautomerization was proposed as the key step in reaction pathway. When using the TiO₂ and ZrO₂ supports, chemoselective hydrogenation of C=O group in the tautomer (methylcyclohexadienone) was enhanced by the oxophilic sites (i.e., Ti⁰⁺ and Zr⁰⁺) to form the methylcyclohexadienol, which was readily dehydrated to toluene on the acid site. As a result, the arene selectivity reached up to 88% and 67% on Pt/TiO₂ and Pt/ZrO₂, respectively. The effects of support and reaction condition were studied by Griffin et al.¹⁴⁶ using HDO of cresol as modelling reaction. The DFT results showed that the direct ring hydrogenation over Pt (111) had the minimum energy barrier, while TiO₂ mainly catalyzed the DDO and partial hydrogenation of cresol followed by dehydration at high temperature (e.g. 350 °C). When Pt was supported on TiO₂, H₂ spillover facilitated the oxygen vacancies formation to catalyze the deoxygenation. This synergy between hydrogenation catalyst (i.e. Pt) and reducible metal oxide support (i.e. TiO₂) could enhance the production of toluene such that Pt/TiO₂ displayed much higher aromatic selectivity than monometallic Pt/C. Together with the thermodynamically favorable conditions (i.e., higher temperature and lower H₂ pressure) a toluene selectivity of 78% was obtained on Pt/TiO₂ at 350 °C and 5 bar H₂. Wang et al.¹⁶⁶ compared the HDO of cresol on Pt/C and Pt-WO_x/C. The Pt-WO_x/C shows much higher conversion (61%) than Pt/C (8.3%) and 98% selectivity to toluene at 300 °C and 36 bar pressure as shown in Figure 16. The close interaction between Pt and WO_x lowered the barrier to form oxygen vacancies, on which hydroxyl group of cresol was bonded with the aromatic ring being oriented away from the Pt. Consequently, direct cleavage of the C-O bond was promoted, as confirmed by the experimental results and DFT calculation. Sn is another metal that promotes the performance for selectively producing the arenes. The bimetallic Pt-Sn displayed higher activity and stability than monometallic Pt and Sn catalysts¹⁶⁷. However, the reaction conditions employed in this study (400 °C and 1 bar) thermodynamically favor the arene production, the comparisons about selectivity were ambiguous. The Pt-based and Rh-based catalysts were also evaluated for the conversion of oligomeric technical lignin with average molecular weight centered at 1710 – 2590 Da¹¹⁷. Among various combination of noble metals and solid acid supports (NH₄⁺ Z-Y zeolite), the Pt/Al₂O₃ and Rh/Al₂O₃ displayed 66%-70% toluene selectivity. The high selectivity to toluene was ascribed to the vertical adsorption of phenolic intermediate on the Al₂O₃ support.

Other noble-metal-based catalysts have also been reported to display high arene selectivity. The ReO_x supported by carbon nanofiber was evaluated for HDO at 300 °C and 30 bar, showing ~72% selectivity to benzene¹⁶⁸. The characterization including XPS of fresh and spent catalysts suggested that it was the *in situ* generated oxygen vacancies that catalyzed the HDO reaction and exhibited preferred DDO of phenol to benzene. The mechanism involved the coordinatively unsaturated Re⁴⁺ interacting with oxygen in phenol, proton transfer to form phenoxide ion, C-O bond cleavage and regeneration of oxygen vacancies by H₂O elimination. These researchers further studied the effect of partially reduced MoO_x and VO_x on the Re catalysts in the HDO of anisole¹⁶⁹, which significantly increased the arene selectivity from ~20% to >50%. The promotion effect was attributed to the enhanced adsorption of anisole on oxygen vacancies of MoO_x and VO_x. The Re-Ni bimetallic catalyst was also reported showing the synergy with Re adsorbing O atom and Ni adsorbing phenyl ring, which facilitated deoxygenation to toluene. Compared with monometallic Ni, Re-Ni showed improved toluene selectivity in the HDO of cresol³⁹, due to the enhanced DDO rate. In

addition, Re addition reduced the electronic density in d states of Ni weakening the adsorption of the aromatic ring, which also likely inhibited the ring saturation.

To summarize this part, two key factors have been generally accepted to influence the selectivity of noble-metal-based catalysts, namely the adsorption configuration of phenolic compounds and the oxophilic properties of additives/supports. One remaining open question for further discussions is whether the oxophilic additives/supports would change the adsorption configuration, or both are essentially doing same synergic chemistry but interpreted from two different angles. Additives/supports that have been widely reported to enhance the noble-metal-based catalysts include WO_x , NbO_x , TiO_x and Fe. However, the role of the oxides/metals in promoting the selectivity is still in debate. For instance, WO_x on Pt substrate was found to tilt the aromatic ring away from Pt to inhibit the hydrogenation of aromatic ring but the high oxophilicity caused by WO_x is demonstrated to promote the DDO reaction rate¹⁶⁶. On the Ru- WO_x catalyst, the high arene selectivity was attributed to oxophilicity of WO_x , rather than adsorption geometry¹⁵⁶. Another comparison study modifying Pt surface with Zn¹⁵¹, which has low oxophilicity¹⁷³, demonstrated that the adjusted adsorption of anisole from parallel configuration to vertical one is the key factor that lowered the ring saturation activity. While Ru over different supports display distinct C-O bond cleavage energies and arene selectivity even with the same vertically adsorbing configuration¹⁵⁵, it suggests one selectivity promoter may play both roles, i.e. adjusting adsorption configuration and oxophilicity, over HDO catalysts to increase the arene selectivity.

4.4 Metal carbides, nitrides and phosphide

4.4.1 Overview of carbides, nitrides and phosphides: structural properties and catalytic performances

Metal carbides, nitrides and phosphides exhibit similar physical properties as metals and ceramics¹⁷⁴. They are catalytically active for many hydrogen-involved reactions such as: CO hydrogenation¹⁷⁵, ammonia synthesis¹⁷⁶, neopentane hydrogenolysis¹⁷⁷, etc. Carbides can be classified as covalent, ionic and interstitial types, with SiC, CaC_2 and WC as the representative of each type¹⁷⁸. Among the three categories, the interstitial one is the most commonly utilized HDO catalyst. In 1970s, Levy et al.¹⁷⁹ reported that formation of tungsten carbide affected the electronegativity of tungsten, making the new species behave like platinum in catalyzing the reaction of H_2 and O_2 . This observation motivated great interests in the following exploration of the carbides' catalysis which have been ascribed to the modification of d-band occupation and Fermi level of the metal by carbon¹⁷⁸. Similar to the interstitial carbides, the nitrides are formed with nitrogen atoms residing in the interstitial spaces between the host metal atoms, forming crystal structures like face-centered cubic, simple hexagonal and hexagonal closed-packed¹⁸⁰. The formed metal nitrides are also described as having similar catalytic performance as noble metals.¹⁷⁹ For phosphides, however, phosphorus atom is usually located at the center of triangular prism since the radius of phosphorus is considerably larger than carbon and nitrogen, making it unstable in octahedral coordination¹⁸⁰. The detailed structures of these materials have been well summarized elsewhere^{174, 178, 181, 182}, and those will not be discussed in this review.

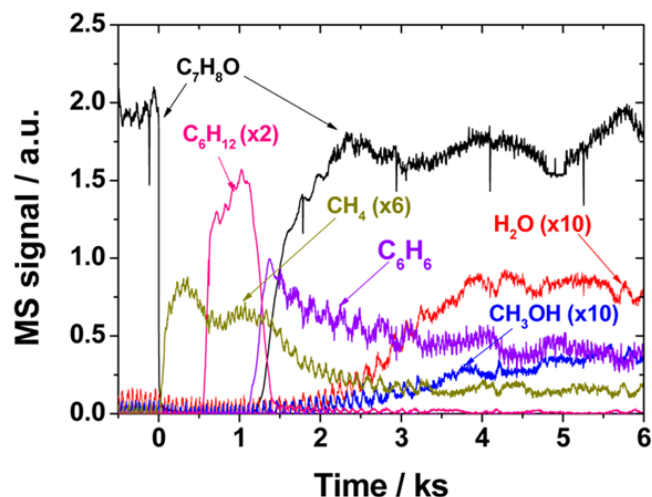


Figure 17. Transient mass spectrometer (MS) signals of the products in HDO of anisole over Mo_2C tested in the vapor phase anisole HDO reaction at ~ 423 K under ambient pressure. Reprinted with permission from Lee et al.¹⁹⁷ Copyright (2015) American Chemical Society.

Applications of carbides, nitrides and phosphides catalysts in hydroprocessing (HDS, HDN, etc.) can be dated back decades ago. Ramanathan et al.¹⁸³ evaluated a series of transition metal carbides and nitrides in hydrotreatment of model compound mixtures and showed that these materials could be promising hydrogenation catalysts. In the meantime, Robinson et al.¹⁸⁴ investigated a group of transition metal phosphides that showed outstanding HDN activity. Since then, more and more researches have been devoted to the applications of carbides, nitrides and phosphides in hydroprocessing^{181, 185, 186}. Inspired by their catalytic performance in HDS and HDN, HDO over the catalysts (C/N/P) have received extensive attentions for the past decade. Several recent papers have well reviewed the metal carbide catalysts for biomass valorization.^{182, 187-189} In these literatures, two interstitial carbides (i.e. MoC_x and WC_x) were discussed in the HDO of lignin-derived phenols and other oxygenates, with main focus on and the synthesis methods of the carbides and reaction mechanisms. Herein, we mainly highlight the factors that contribute to the improved selectivity. Transition metal phosphides, such as FeP_x , CoP_x , NiP_x , MoP_x , WP_x , as well as the bimetallic phosphide, have also been studied as HDO catalysts¹⁹⁰⁻¹⁹². The P ligand can form surface P-OH group with acidity¹⁹³ to catalyze dehydration of the partially hydrogenated enol from phenolics to produce arene¹⁶⁴. Nitride catalysts studied for HDO are not as many as those of carbides and phosphides. The reported nitrides include MoN_x , WN, VN, NbN and TiN et al.^{183, 194}.

4.4.2 Selective carbide, nitride and phosphide catalysts

Although the general approaches to promote the arene selectivity has not been adequately established for carbides/nitrides/phosphides, certain catalysts have displayed high arene selectivity in HDO of phenolics (Table 6). Lee et al.¹⁹⁵ applied Mo_2C for the anisole HDO at low temperature (147°C - 247°C) and ambient pressure. The catalyst displayed $>90\%$ arene selectivity which was attributed to the inhibition of the hydrogenation functionality of catalyst by the *in situ* generated oxygen-containing species (surface oxycarbide formed by abstracting the O in anisole).

A similar study for HDO of phenolic mixture was also reported showing >90% arene selectivity on Mo₂C¹⁹⁶. Based on the results of *in situ* methanol and/or water titration of benzene/toluene hydrogenation, modification of the catalyst surface by oxygenates was proposed as the major cause for the inhibited ring saturation. Active sites for selective deoxygenation of anisole using chemical titration and transient kinetics were later on studied¹⁹⁷. As shown in Figure 17, no oxygenate but only cyclohexane was initially observed right after the anisole/H₂ mixture was introduced into the reactor, suggesting the initial oxygenates' accumulation (~0.29 monolayer) on the catalyst surface. With time on stream, oxygenates were observed in the outlet. Meanwhile, benzene was detected which increased at the expense of cyclohexane. Temperature-programmed surface reaction with H₂ of spent Mo carbide catalyst (without exposure to air) produced oxygen-containing species such as H₂O, CO, CO₂ and methanol. This result indicated that the generated surface oxygen species on Mo₂C might have suppressed the ring saturation and thus increased arene selectivity. Mo₂C was also pretreated with different oxygenates (H₂O, CO₂, O₂) to study the influence of surface oxygen on the catalytic performances in HDO of m-cresol¹⁹⁸. Oxygen uptake measured from TPSR was found to correlate with toluene formation rate. The turnover frequencies based on CO titration of catalysts pretreated with different oxygenates were similar. This implied that the effect of adsorbed

oxygen was independent of the oxygen source. The surface chemistry of Mo₂C during HDO reaction was also studied by Murugappan et al.¹³⁸ with operando NAP-XPS. The spectra in C and O regions suggested the presence of both surface carbidic and oxycarbide species. The formation of oxycarbide species was an indication of surface oxidation of carbide (Mo²⁺) to other oxidic Mo species (i.e., Mo⁵⁺ and Mo⁶⁺). Together with the improved reactivity (comparing with oxide) along with the formation of oxycarbide species, it was proposed that the carbide/oxycarbide was responsible for the HDO over Mo₂C. This is aligned with their previous study⁵⁷ on MoO₃ where the oxycarbide formation is observed in the induction period, and was correlated with the enhanced activity. It was also proposed that oxycarbide might help to maintain the Mo⁵⁺ oxidation state to catalyze the reaction. The spectra for C 1s showed the carbonaceous deposits grew during reaction, indicating coking was probably the main reason for the deactivation. Carbides and oxycarbides were also studied by Wang et al.¹⁹⁹ with Mo₂C-MoC_xO_y supported on active carbon, displaying >70% arene selectivity in the HDO of cresol at 350 °C and 4.3 MPa. XPS results confirmed the presence of Mo₂C and MoO_xC_y phases. The kinetics (apparent activation energy for DDO and HYD and reaction rate) had no strong correlations with the Mo₂C/MoC_xO_y ratio, suggesting both phases may serve as the active sites.

Table 6. Catalytic performances of carbides, nitrides and phosphides with high arene selectivity for the HDO of model compounds.

Catalyst	Reaction condition			Substrate	Conv. (%)	S _{arene} (%)	Ref
	T(°C)	P (bar)	Solvent/Reactor ^a				
Mo ₂ C	150	1	-/c	Anisole	~10~19	~95	197
Mo ₂ C	150	1	-/c	Anisole	<14	90-94	195
Mo ₂ C	150	1.1	-/c	Anisole	~40	80	200
W ₂ C	171	1.3	-/c	Anisole	~20	96	200
O ₂ -0.05kPa-Mo ₂ C	150	1	-/c	Cresol	~18	95	198
O ₂ -1kPa-Mo ₂ C	150	1	-/c	Cresol	~1.5	91	198
H ₂ O-1kPa-Mo ₂ C	150	1	-/c	Cresol	~18	96	198
CO ₂ -1kPa-Mo ₂ C	150	1	-/c	Cresol	~8.7	96	198
Mo ₂ C	150	1	-/c	Cresol	21	95	198
Mo ₂ C	280	1.1	-/c	Phenolic mixture	94	93	196
MoC-SiO ₂	320	60	Hexadecane/b	Anisole	~65	~70	201
MoC ₂	250	1	-/c	Anisole	49	~87	202
MoC ₂	350	4.4	-/c	Guaiacol	99.8	~81	59
MoC _x O _y /Carbon	325	43	Decalin	Cresol	~25	~70	199
Mo ₂ C/TiO ₂	350	25	Decane/c	Phenol	~65	~90	134
Mo ₂ N/TiO ₂	350	25	Decane/c	Phenol	~9	~91	134
MoP/TiO ₂	350	25	Decane/c	Phenol	~25	~82	134
Ni ₂ P/SiO ₂	300	1	-/c	Guaiacol	80	60	191
Co ₂ P/SiO ₂	300	1	-/c	Guaiacol	32	52	191
MoP/SiO ₂	300	1	-/c	Guaiacol	54	53	191
Ni ₂ P/SiO ₂	300	1	Tridecane/c	Guaiacol	85	62	203
Ni ₂ P/SiO ₂	300	1	-/c	Guaiacol	55	86	204
Ni ₂ P/SiO ₂	300	1	-/c	Anisole	71	81	204
Ni ₂ P/SiO ₂	400	15	-/c	Anisole	100	60.6	205

MoP-CA	350	44	Decalin/b	Cresol	58	60	206
FeMoP	400	21	Decalin/b	Phenol	>99	90	60
FeMoP	350	21	Decane/b	Phenol	63	70	60

^a b: batch reactor; c: continuous flow reactor.

Lu et al.²⁰⁰ prepared the ordered mesoporous Mo₂C and W₂C by the hard template method. These catalysts are among the scarce examples of mesoporous carbides with very large surface area for HDO reaction. At ambient pressure and low reaction temperature (i.e., 150 °C for Mo₂C and 170 °C for W₂C) anisole was deoxygenated to arenes with selectivity of 80% and 96%, respectively. The higher arene selectivity for W₂C than Mo₂C at such a low reacting temperature was ascribed to the stronger oxygen affinity of W. However, the TOF of W₂C based on by CO titration (adsorbing on the metal-like active sites) is much smaller than that of Mo₂C, which might be attributed to the extremely high oxophilicity of W retarded the redox cycle for catalytic HDO (the detailed discussion is presented in section 5). Iida et al.²⁰² encapsulated MoC_x nanocluster inside the pores of zeolites with faujasite (FAU) topology, and used the bifunctional catalyst for vapor-phase HDO of anisole as shown in Figure 18. The largest benefit provided by this catalyst was the promoted alkylation with high aromatic selectivity, which preserved the carbon in the desirable products. The formation of alkylated aromatics was attributed to the transalkylation of methoxy groups from one anisole molecule to another by Brønsted acid sites in close vicinity to the MoC_x species in the MoC_x/FAU catalysts. Comparing with the physically mixed Mo₂C and FAU, the bifunctional MoC_x/FAU displayed significantly improved stability within 20h of time-on-stream reaction. Besides the vapor-phase reaction, MoC_x has also been investigated in the liquid-phase reaction. Smirnov et al.²⁰¹ prepared the MoC_x-SiO₂ and bimetallic NiMoC_x-SiO₂ for the HDO of anisole. The MoC_x-SiO₂ converted anisole to benzene with ~70% selectivity at 320 °C and 60 bar pressure. The kinetic study showed that reaction pathway involved the direct C-O bond cleavage to C_{aromatic}-OCH₃ bond forming benzene, rather than via the phenol intermediate. Using Ni as the promotor (presenting both on the catalyst surface and in the carbide particles) increased the activity toward ring saturation, making the bimetallic catalysts less selective (i.e. arene selectivity was 3%-40% depending on the variation of Ni content).

The application of nitrides in HDO of phenols are not as extensive as that of carbides. Several researchers studied the nitride catalysts (e.g. MoN_x, CoMoN_x) with guaiacol as the model compound, which

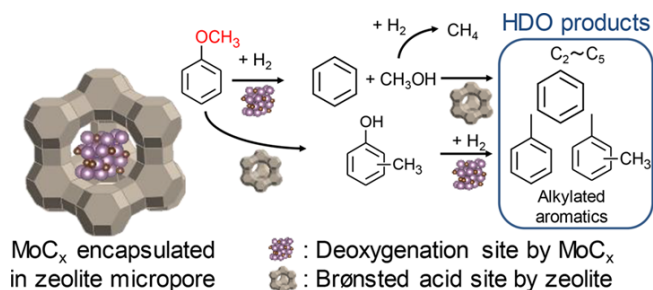


Figure 18. Anisole conversion by MoC_x encapsulated FAU zeolite catalyst for producing alkylated aromatics and C₂~C₅ light gas elements by the combination of zeolitic Brønsted acid sites and MoC_x deoxygenation sites. Reprinted with permission from Iida et al.²⁰² Copyright (2017) American Chemical Society.

was partially deoxygenated to other phenols^{207, 208}. This makes it difficult to directly compare the arene selectivity. Ghampson et al.²⁰⁹ also studied Mo₂N and CoMoN_x catalysts in the HDO of guaiacol. These nitrides directly cleave the C_{aromatic}-OCH₃ bond in guaiacol forming phenol, but then saturate the ring during HDO process to form cyclohexene and cyclohexane at 300 °C and 50 bar H₂ pressure. However, the product distribution can be adjusted by applying the oxophilic support. For example, when Mo₂N is supported on TiO₂, the catalyst displayed ~91% arene selectivity in the HDO of phenol at 350 °C and 25 bar total pressure¹³⁴. Ghampson et al.²¹⁰ compared two different supports for MoN_x-catalyzed HDO of guaiacol. MoN_x/Al₂O₃ mainly transformed guaiacol to catechol by demethylation, while the MoN_x/SBA-15 converted guaiacol to phenol by directly removing the methoxy group, which was a more efficient deoxygenation pathway to eventually obtain the arene products. This might be due to the formation of γ-Mo₂N crystalline phase on SBA-15 (whereas Al₂O₃ support led to small crystallites of nitrides) that led to the higher activity in direct cleavage of C_{aromatic}-OCH₃ bond. No correlation between activity and relative content of nitride/oxynitride was discovered, implying multiple active phases might catalyze the guaiacol conversion.

As one class of hydroprocessing catalysts, transition metal phosphides are another group of potential candidates for HDO of phenols. The pioneer study has shown that MoP has the higher activity, lower activation energy and high arene selectivity comparing with its sulfide and oxide counterparts⁸⁷. Following that, a series of phosphide catalysts including Fe₂P/SiO₂, Co₂P/SiO₂, Ni₂P/SiO₂, MoP/SiO₂ and WP/SiO₂, were tested in the vapor-phase HDO of guaiacol at 1 bar and different temperatures¹⁹¹. Among the catalysts tested, Ni₂P/SiO₂ displayed the highest turnover frequency and benzene selectivity (60%). The kinetic measurements showed the apparent activation energy of 40 kJ/mol for Ni₂P/SiO₂, which is lower than that of the direct C-O bond cleavage, implying that the enhanced benzene formation was from the hydrogenation of C=C double bonds in the aromatic ring followed by dehydration. The HDO properties of Ni₂P/SiO₂ were also studied by Moon et al.²⁰³ using guaiacol as the model compound at different reacting conditions. Reaction pressure was found to largely determine the reaction pathway and product distribution: DDO to benzene dominated (62% selectivity) at 1 bar and 300 °C while HYD to produce cyclohexane (benzene selectivity is 8%) prevailed at 8 bar pressure. This observation is consistent with other studies showing that

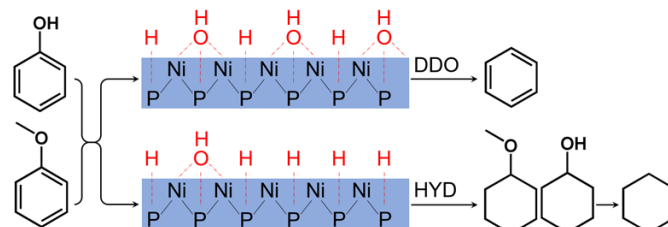


Figure 19. The proposed reaction pathways of guaiacol HDO over Ni₂P catalyst: product distribution is dependent on the densities of surface OH group and more reduced metal sites.²⁰³

dicyclohexane was main O-free product in HDO of dibenzofuran at 30 bar pressure,²¹¹ and ring saturation is favored in HDO of anisole at lower temperature and higher H₂ pressure and vice versa²⁰⁵. Further XAFS measurement revealed the slightly oxidized surface on the spent catalyst tested at 1 bar, and DFT calculations showed that both H and OH were able to adsorb on unsaturated threefold hollow (TFH)-Ni site. Based on their results, it was proposed that the DDO pathway was favored by the surface OH groups, while HYD pathway was favored on more reduced surface. Therefore, arene selectivity could be tuned by the relative populations of H and OH groups on the surface, as shown in Figure 19. Lan et al.²⁰⁴ studied the HDO reactions on Ni₂P/SiO₂ catalysts at 300°C and 1 bar using guaiacol and anisole. Guaiacol and anisole were deoxygenated to benzene with 86% and 81% selectivity, respectively. Benzene selectivity decreased and phenols selectivity increased as the reaction time proceeded. This gradual change was accompanied with the increase of Ni^{δ+}+Ni⁰ amount and the decrease of P/Ni ratio. Ni^{δ+} was proposed as Lewis acid site to catalyze the demethylation rather than demethoxylation, and Ni⁰ only showed low reactivity for dehydroxylation. In addition, decrease of P/Ni ratio reduced the amount of Brønsted acid sites so that the dehydroxylation was suppressed. These factors jointly led to the decrease of benzene selectivity.

Besides NiP_x, MoP_x is another series of phosphide reported for the HDO reaction. Whiffen et al.²⁰⁶ prepared the MoP with the addition of citric acid (MoP-CA) which generated residual C on the catalyst and hence mitigated the agglomeration of the formed MoP nanoparticles (i.e., 5-9 nm). Compared with the MoP prepared in the absence of citric acid, MoP-CA displayed promoted activity and toluene selectivity (60% vs 49%). It is proposed that the MoP-CA has less highly reduced and weak electrophilic sites on which HYD occurs, and thus inhibiting ring saturation. MoP could be further modified by Fe on the bimetallic phosphide FeMoP, which showed much higher arene selectivity than monometallic FeP, MoP, and a physical mixture of FeP+MoP in the HDO of anisole⁶⁰. HDO of several model compounds (i.e., anisole, phenol, 2-phenoxyethyl benzene) showed that ring saturation with FeMoP could be inhibited by decreasing H₂ concentration or using high reaction temperatures. In the following investigation²¹², a correlation was discovered that the catalyst with higher amount of P vacancies showed enhanced selectivity to arene even at high conversion of phenol. This was possibly due to vacancy bond to the hydroxyl group in phenol to destabilize the C-O bond to achieve the selective C-O bond cleavage.

5. Perspective

The challenge of HDO of phenolics is to achieve both elimination of oxygen and preservation of aromatic ring (i.e., DDO pathway) in order to minimize hydrogen consumption and to increase the octane number of the products. With numerous efforts, several efficient strategies have been developed and demonstrated for the DDO of phenolics, including catalyst design (e.g., oxophilicity of the catalysts), reaction engineering control (e.g., different thermodynamics/kinetic regime and reaction mechanism in gas phase vs liquid phase), or a combination of both. Note that some catalysts, being selective in vapor-phase reaction, dramatically lose the selectivity in liquid-phase reaction^{69, 213}. This distinct

performance, as abovementioned, could be caused by the different control of thermodynamics/kinetics under different reacting conditions, change of surface adsorption configuration or surface reaction mechanisms. A definitive answer still requires further investigations to fully obtain the insights, which will provide the guidance for the design of selective HDO catalysts/processes. To this end, our recent studies on PdFe catalysts, comparing the HDO of phenolics in vapor-phase vs liquid-phase reactions⁶², revealed that, despite of the highly selective DDO of phenolics on PdFe in vapor-phase reaction conditions, a much facile tautomerization reaction pathway was opened up in liquid-phase reaction conditions, leading to the dominant aromatic ring saturation. Though it remains ambiguous in terms of what caused the enhanced tautomerization pathway, this study suggests that suppressing tautomerization may improve the catalyst selectivity under the liquid-phase conditions.

Although the anionic ligand in a catalyst can alter the electron density and thus catalytic properties of the metal^{192, 214}, its effect to arene selectivity seems limited. In the comparative studies of metal sulfide, oxide, carbide, nitride and phosphide, regardless of anionic ligand used, while Mo-based catalysts display high arene selectivity (>50%)^{87, 134}, Ni-based catalysts (i.e., metallic^{31, 201}, sulfide¹⁰³ or phosphide^{215, 216}) mainly saturate the aromatic ring in the liquid-phase reaction conditions (i.e., high hydrogen pressure). Another factor that may lead to their similar selectivity is the surface reconstruction, namely, regardless of the as-synthesized phase of catalysts, the surface may eventually change into a similar structure in HDO reaction conditions. For instance, oxycarbide species, which are probably necessary for selective HDO¹³⁸, appeared on both MoO₃⁵⁷ and Mo₂C¹⁹⁷ catalysts as the reaction processed. Understanding the nature of metals may be essential to design selective HDO catalyst.

Other than the anionic ligand, oxophilicity of metals is a key descriptor that had been extensively studied. Since the reported data were obtained over a wide range of reacting conditions, it is impossible to make a quantitative comparison of the catalysts. However, we qualitatively cross-compare the catalytic performances of each monometallic catalyst reported in the literatures^{30, 40, 122, 123, 127, 146, 148, 149, 155, 156, 168, 217-219}. As shown in Figure 20a, a clear trend is present, i.e., arene selectivity for HDO of phenols increases with oxophilicity index from 0 (with Pd as representative) to 0.6 (with Mo as representative). Further increase of oxophilicity (with Ti, Ce as representative) dramatically decreases the reactivity (Figure 20b). Based on their oxophilicities, the metals are divided into three groups, namely low (0 – 0.3), moderate (0.4 – 0.7) and high (0.8 – 1) oxophilicity. From the above correlations, low oxophilic metals are not active enough to abstract O to achieve direct C-O bond cleavage but show high activity to saturate the aromatic ring; whereas the high oxophilic metals tend to strongly interact with the abstracted O, making it difficult to release the O even in the presence of H₂ such that the redox cycle cannot be completed. Only the metals with moderate oxophilicity is able to not only abstract the O from the phenolics but readily eliminate it with the help of H₂ making those catalysts good candidates for HDO. A similar conclusion was also drawn on oxide catalysts by Goulas et al.²²⁰ who reported a volcano-type dependence of reaction rate for C-O bond cleavage in furfural on the Gibbs free energy of metal oxide formation (another way to evaluate the oxophilicity of metal). This correlation²²⁰ for oxide catalysts originated from the reverse Mar-van Krevelen C-O bond

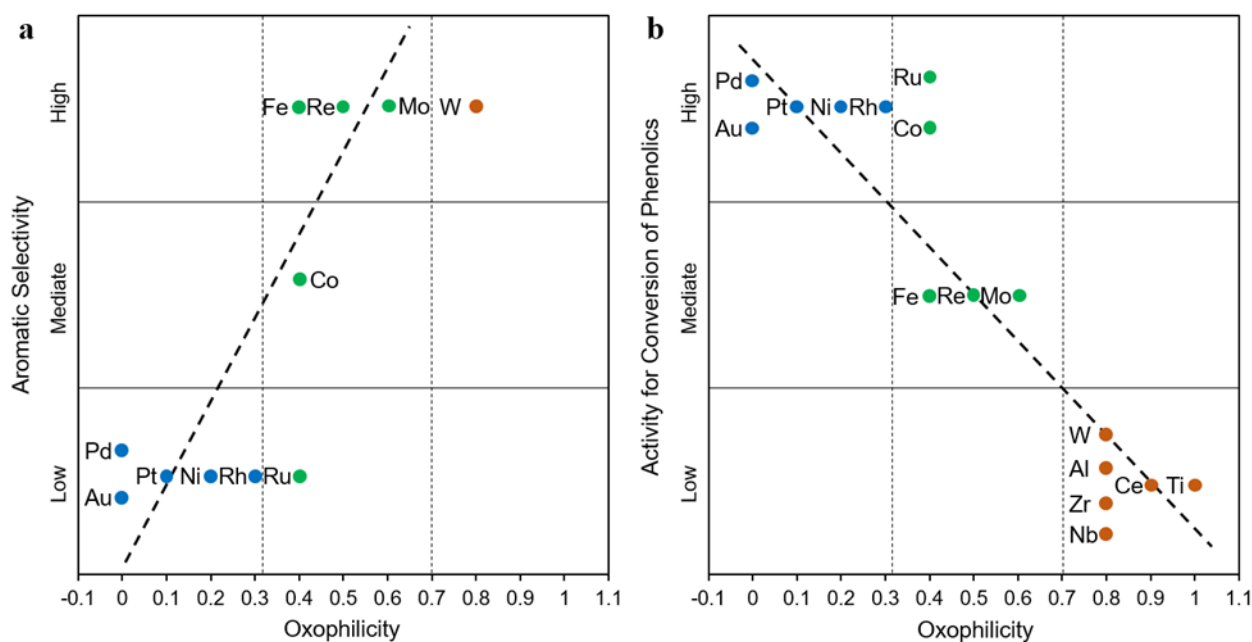


Figure 20. A qualitative summary about the relation between arene selectivity (a), activity for conversion of phenols (b) in HDO with oxophilicity of the monometallic species. The oxophilicity is referred from the literature¹⁷³.

activation mechanism, which needs a trade-off between the O abstraction and elimination on the vacancy site.

As mentioned above, elimination of the abstracted O is essential to close the redox cycle during the HDO reactions, other than using moderate oxophilic metals, the combination of low/moderate, low/high and moderate/high oxophilic metals to form bifunctional catalysts is another potential approach for selective HDO, with Pd-Fe^{123, 124}, Ru-NbO_x¹⁵⁵, Ru-WO_x¹⁵⁶, Pt-WO_x¹⁶⁶, Ru-TiO₂¹⁵⁷, Pd-NbO_x¹⁶¹ etc. as examples. Over these catalysts, it is proposed that the highly oxophilic metal species abstract the O atom to cleave the C-O bond and the low oxophilic metals activate the H₂ to facilitate the redox cycle. This also implies the potential application of single-atom catalysts, i.e. low oxophilic metals with atomic dispersion on highly oxophilic support. By atomic dispersion, both oxophilicity of support and H₂-activation capacity of guest metal are tuned, and more importantly the nature of low oxophilic metals is changed (i.e., support modifies the property of atomically dispersed metal) so that the direct ring-hydrogenation is inhibited. However, one barrier that needs to overcome is the aggregation^{221, 222} of the low oxophilic metals especially in reduction atmosphere at HDO temperature (usually above 250 °C)²²³. The reduction and aggregation will create identity of low oxophilic metals (i.e., large metal particles showing intrinsic property similar/same as the bulky metal) that decrease the HDO selectivity. For the metals not included in Figure 20, one can find the oxophilicity index of a specific metal in ref¹⁷³.

Majority of current HDO of phenolics focuses on the structure of catalyst or mechanism. The effect of water or solvent (regarding to mechanism and performance) have yet been fully understood. In fact, promising results have been shown to control arene selectivity by applying the solvent effect or using water as co-catalyst^{10, 157, 224, 225}. For example, water additive significantly promoted the arene selectivity of Ru/TiO₂, and water was proposed to lower the barrier for C-O cleavage¹⁵⁷. Whereas, another possibility could be the

presence of water stabilizes the highly dispersed Ru single atom/clusters against the formation of large Ru particles so that the high arene selectivity is achieved. Moreover, applying water as solvent has been reported to provide alternative reaction pathway in hydroprocessing²²⁶. Overall, further study about effect from water or solvent to arene selectivity is needed. Another species that needs more investigation in phenolic HDO is alkali, which is usually reported with negative impact to HDO catalysts^{72, 73}. However, alkali-metal species has been proved as a promising promoter in C-O bond cleavage of aryl ethers²²⁷⁻²²⁹. In these studies, base additive such as sodium tert-butoxide (NaO^tBu) inhibits the ring saturation to make the catalytic system selectively produce aromatics²²⁷⁻²²⁹, which is a valuable inspiration for development of phenolic HDO catalysts. Finally, despite of the extensive studies, majority of those are still focused on using model compounds (aromatic oxygenates or simulated mixtures). Applications of the selective catalysts discussed in real bio-oil are still quite limited. However, several catalysts reported recently have been shown promising in the process of real bio-oil, including PtFe-C/SiO₂²³⁰ for pyrolysis-oil vapor, Fe/SiO₂¹³⁶ for lignin pyrolysis vapor, Ru/Nb₂O₅ for real lignin¹⁵⁵, Pt/Al₂O₃ NH₄⁺ Z-Y and Rh/Al₂O₃ NH₄⁺ Z-Y¹¹⁷ for oligomeric technical lignin, etc. Future work needs to further deepen the fundamental insights that guide catalyst design for practical application of the selective HDO catalysts in the real bio-oil upgrading.

Conflicts of interest

There are no conflicts to declare.

Acknowledgements

This work was supported by the U.S. Department of Energy (DOE), Office of Science, Basic Energy Sciences (BES) and

Division of Chemical Sciences, Biosciences and Geosciences (grant DE-FG02-05ER15712; DE-AC05-RL01830, FWP-47319).

Notes and references

- A. D. Sutton, F. D. Waldie, R. Wu, M. Schlaf, L. A. Silks, 3rd and J. C. Gordon, *Nat. Chem.*, 2013, **5**, 428-432.
- D. King and C. Grey, *Energy Harnessing: New Solutions for Sustainability and Growing Demand*, World Economic Forum, CH-1223 Cologny/Geneva, Switzerland, 2013.
- S. Crossley, J. Faria, M. Shen and D. E. Resasco, *Science*, 2010, **327**, 68-72.
- Y. Roman-Leshkov, J. N. Chheda and J. A. Dumesic, *Science*, 2006, **312**, 1933-1937.
- C. Li, X. Zhao, A. Wang, G. W. Huber and T. Zhang, *Chem. Rev.*, 2015, **115**, 11559-11624.
- D. D. Laskar, B. Yang, H. Wang and J. Lee, *Biofuel. Bioprod. Biorefin.*, 2013, **7**, 602-626.
- X. Li, G. Chen, C. Liu, W. Ma, B. Yan and J. Zhang, *Renew. Sust. Energ. Rev.*, 2017, **71**, 296-308.
- G. W. Huber, S. Iborra and A. Corma, *Chem. Rev.*, 2006, **106**, 4044-4098.
- D. M. Alonso, S. G. Wettstein and J. A. Dumesic, *Chem. Soc. Rev.*, 2012, **41**, 8075-8098.
- X. Wang and R. Rinaldi, *ChemSusChem*, 2012, **5**, 1455-1466.
- H. Wang, H. Ruan, M. Feng, Y. Qin, H. Job, L. Luo, C. Wang, M. H. Engelhard, E. Kuhn, X. Chen, M. P. Tucker and B. Yang, *ChemSusChem*, 2017, **10**, 1846-1856.
- A. J. Ragauskas, G. T. Beckham, M. J. Bidy, R. Chandra, F. Chen, M. F. Davis, B. H. Davison, R. A. Dixon, P. Gilna, M. Keller, P. Langan, A. K. Naskar, J. N. Saddler, T. J. Tschaplinski, G. A. Tuskan and C. E. Wyman, *Science*, 2014, **344**, 1246843.
- Q. Bu, H. Lei, A. H. Zacher, L. Wang, S. Ren, J. Liang, Y. Wei, Y. Liu, J. Tang, Q. Zhang and R. Ruan, *Bioresour. Technol.*, 2012, **124**, 470-477.
- S. Laurichesse and L. Avérous, *Prog. Polym. Sci.*, 2014, **39**, 1266-1290.
- S. L. Yohe, H. J. Choudhari, D. D. Mehta, P. J. Dietrich, M. D. Detwiler, C. M. Akatay, E. A. Stach, J. T. Miller, W. N. Delgass, R. Agrawal and F. H. Ribeiro, *J. Catal.*, 2016, **344**, 535-552.
- L. Chen, J. Xin, L. Ni, H. Dong, D. Yan, X. Lu and S. Zhang, *Green Chem.*, 2016, **18**, 2341-2352.
- J. He, C. Zhao and J. A. Lercher, *J. Am. Chem. Soc.*, 2012, **134**, 20768-20775.
- M. Saidi, F. Samimi, D. Karimipourfard, T. Nimmanwudipong, B. C. Gates and M. R. Rahimpour, *Energ. Environ. Sci.*, 2014, **7**, 103-129.
- A. L. Jongorius, R. Jastrzebski, P. C. A. Bruijninx and B. M. Weckhuysen, *J. Catal.*, 2012, **285**, 315-323.
- X. Wang and R. Rinaldi, *Catal. Today*, 2016, **269**, 48-55.
- M. Tian, R. L. McCormick, M. A. Ratcliff, J. Luecke, J. Yanowitz, P.-A. Glaude, M. Cuijpers and M. D. Boot, *Fuel*, 2017, **189**, 284-292.
- D. C. Elliott, *Energ. Fuel*, 2007, **21**, 1792-1815.
- K. Routray, K. J. Barnett and G. W. Huber, *Energy Technol.*, 2017, **5**, 80-93.
- H. Xu, B. Yu, H. Zhang, Y. Zhao, Z. Yang, J. Xu, B. Han and Z. Liu, *Chem. Commun.*, 2015, **51**, 12212-12215.
- X. Wang and R. Rinaldi, *Angew. Chem. Int. Ed.*, 2013, **52**, 11499-11503.
- H. Sajiki, A. Mori, T. Mizusaki, T. Ikawa, T. Maegawa and K. Hirota, *Org. Lett.*, 2006, **8**, 987-990.
- M. Tobisu, K. Yamakawa, T. Shimasaki and N. Chatani, *Chem. Commun.*, 2011, **47**, 2946-2948.
- Y. Pan and C. P. Holmes, *Org. Lett.*, 2001, **3**, 2769-2771.
- J. A. Anderson, B. K. Lin, H. J. Williams and A. I. Scott, *J. Am. Chem. Soc.*, 1988, **110**, 1623-1624.
- T.-S. Nguyen, D. Laurenti, P. Afanasiev, Z. Konuspayeva and L. Piccolo, *J. Catal.*, 2016, **344**, 136-140.
- C. Zhao, Y. Kou, A. A. Lemonidou, X. Li and J. A. Lercher, *Chem. Commun.*, 2010, **46**, 412-414.
- Y. Hong, A. Hensley, J.-S. McEwen and Y. Wang, *Catal. Lett.*, 2016, **146**, 1621-1633.
- V. O. O. Gonçalves, C. Ciotonea, S. Arrii-Clacens, N. Guignard, C. Roudaut, J. Rousseau, J.-M. Clacens, S. Royer and F. Richard, *Appl. Catal. B*, 2017, **214**, 57-66.
- G. Zhu, W. Wang, K. Wu, S. Tan, L. Tan and Y. Yang, *Ind. Eng. Chem. Res.*, 2016, **55**, 12173-12182.
- Y.-R. Lu, *Comprehensive Handbook of Chemical Bond Energies*, Taylor & Francis Group, Boca Raton, Florida, United States., 1st edn., 2007.
- Z. Luo, Z. Zheng, Y. Wang, G. Sun, H. Jiang and C. Zhao, *Green Chem.*, 2016, **18**, 5845-5858.
- R. N. Olcese, M. Bettahar, D. Petitjean, B. Malaman, F. Giovannella and A. Dufour, *Appl. Catal. B*, 2012, **115-116**, 63-73.
- Bioenergy Technologies Office Multi-Year Program Plan: March 2016; U. S. D. o. E. Bioenergy Technologies Office, 2016
- F. Yang, D. Liu, H. Wang, X. Liu, J. Han, Q. Ge and X. Zhu, *J. Catal.*, 2017, **349**, 84-97.
- G. Liu, A. W. Robertson, M. M.-J. Li, W. C. H. Kuo, M. T. Darby, M. H. Muhieddine, Y.-C. Lin, K. Suenaga, M. Stamatakis, J. H. Warner and S. C. E. Tsang, *Nat. Chem.*, 2017, **9**, 810-816.
- E. Furimsky, *Catal. Rev.*, 1983, **25**, 421-458.
- E. Furimsky, *Appl. Catal. A*, 2000, **199**, 147-190.
- H. Wang, J. Male and Y. Wang, *ACS Catal.*, 2013, **3**, 1047-1070.
- Y. Nakagawa, S. Liu, M. Tamura and K. Tomishige, *ChemSusChem*, 2015, **8**, 1114-1132.
- P. Mäki-Arvela and D. Murzin, *Catalysts*, 2017, **7**, 265.
- H. Shafaghat, P. S. Rezaei and W. M. Ashri Wan Daud, *RSC Adv.*, 2015, **5**, 103999-104042.
- C. Xu, R. A. Arancon, J. Labidi and R. Luque, *Chem. Soc. Rev.*, 2014, **43**, 7485-7500.
- A. Agarwal, M. Rana and J.-H. Park, *Fuel Process. Technol.*, 2018, **181**, 115-132.
- S. Wang, B. Ru, H. Lin, W. Sun and Z. Luo, *Bioresour. Technol.*, 2015, **182**, 120-127.
- A. Rahimi, A. Azarpira, H. Kim, J. Ralph and S. S. Stahl, *J. Am. Chem. Soc.*, 2013, **135**, 6415-6418.
- M. P. Pandey and C. S. Kim, *Chemical Engineering & Technology*, 2011, **34**, 29-41.
- R. Prado, A. Brandt, X. Erdocia, J. Hallet, T. Welton and J. Labidi, *Green Chem.*, 2016, **18**, 834-841.
- A. Rahimi, A. Ulbrich, J. J. Coon and S. S. Stahl, *Nature*, 2014, **515**, 249-252.
- L. Shuai, M. T. Amiri, Y. M. Questell-Santiago, F. Heroguel, Y. Li, H. Kim, R. Meilan, C. Chapple, J. Ralph and J. S. Luterbacher, *Science*, 2016, **354**, 329-333.
- B. Güvenatam, O. Kurşun, E. H. J. Heeres, E. A. Pidko and E. J. M. Hensen, *Catal. Today*, 2014, **233**, 83-91.
- Y. Yang, C. Ochoa-Hernández, V. A. de la Peña O'Shea, P. Pizarro, J. M. Coronado and D. P. Serrano, *Appl. Catal. B*, 2014, **145**, 91-100.
- T. Prasomsri, M. Shetty, K. Murugappan and Y. Román-Leshkov, *Energ. Environ. Sci.*, 2014, **7**, 2660-2669.

- 58 R. C. Runnebaum, T. Nimmanwudipong, D. E. Block and B. C. Gates, *Catal. Sci. Technol.*, 2012, **2**, 113-118.
- 59 F. G. Baddour, V. A. Witte, C. P. Nash, M. B. Griffin, D. A. Ruddy and J. A. Schaidle, *ACS Sustain. Chem. Eng.*, 2017, **5**, 11433-11439.
- 60 D. J. Rensel, S. Rouvimov, M. E. Gin and J. C. Hicks, *J. Catal.*, 2013, **305**, 256-263.
- 61 G. H. Gu, C. A. Mullen, A. A. Boateng and D. G. Vlachos, *ACS Catal.*, 2016, **6**, 3047-3055.
- 62 J. Zhang, J. Sun, B. Sudduth, X. Pereira Hernandez and Y. Wang, *Catal. Today*, 2020, **339**, 305-311.
- 63 L. Nie and D. E. Resasco, *J. Catal.*, 2014, **317**, 22-29.
- 64 L. Nie, P. M. de Souza, F. B. Noronha, W. An, T. Sooknoi and D. E. Resasco, *J. Mol. Catal. A*, 2014, **388-389**, 47-55.
- 65 G. Chang, Y. Huang, J. Xie, H. Yang, H. Liu, X. Yin and C. Wu, *Energy Conversion and Management*, 2016, **124**, 587-597.
- 66 A. Centeno, E. Laurent and B. Delmon, *J. Catal.*, 1995, **154**, 288-298.
- 67 D. A. Ruddy, J. A. Schaidle, J. R. Ferrell Iij, J. Wang, L. Moens and J. E. Hensley, *Green Chem.*, 2014, **16**, 454-490.
- 68 C. Wang, G. R. Wittreich, C. Lin, R. Huang, D. G. Vlachos and R. J. Gorte, *Catal. Lett.*, 2019, DOI: 10.1007/s10562-019-03027-8.
- 69 Y. Li, C. Zhang, Y. Liu, X. Hou, R. Zhang and X. Tang, *Energ. Fuel*, 2015, **29**, 1722-1728.
- 70 M. Badawi, J. F. Paul, S. Cristol, E. Payen, Y. Romero, F. Richard, S. Brunet, D. Lambert, X. Portier, A. Popov, E. Kondratieva, J. M. Goupil, J. El Fallah, J. P. Gilson, L. Mariey, A. Travert and F. Maugé, *J. Catal.*, 2011, **282**, 155-164.
- 71 Y. Hong, S. Zhang, F. F. Tao and Y. Wang, *ACS Catal.*, 2017, **7**, 3639-3643.
- 72 P. M. Mortensen, D. Gardini, H. W. P. de Carvalho, C. D. Damsgaard, J.-D. Grunwaldt, P. A. Jensen, J. B. Wagner and A. D. Jensen, *Catal. Sci. Technol.*, 2014, **4**, 3672-3686.
- 73 D. Kubička and J. Horáček, *Appl. Catal. A*, 2011, **394**, 9-17.
- 74 P. M. de Souza, R. C. Rabelo-Neto, L. E. P. Borges, G. Jacobs, B. H. Davis, D. E. Resasco and F. B. Noronha, *ACS Catal.*, 2017, **7**, 2058-2073.
- 75 E. Furimsky and F. Massoth, *Catal. Today*, 1999, **52**, 381-495.
- 76 C. H. Bartholomew, *Appl. Catal. A*, 2001, **212**, 17-60.
- 77 M. Grilc, B. Likozar and J. Levec, *Appl. Catal. B*, 2014, **150-151**, 275-287.
- 78 M. Badawi, J.-F. Paul, S. Cristol and E. Payen, *Catal. Commun.*, 2011, **12**, 901-905.
- 79 W. Wang, K. Zhang, Z. Qiao, L. Li, P. Liu and Y. Yang, *Ind. Eng. Chem. Res.*, 2014, **53**, 10301-10309.
- 80 V. O. O. Gonçalves, S. Brunet and F. Richard, *Catal. Lett.*, 2016, **146**, 1562-1573.
- 81 E. J. M. Hensen, P. J. Kooyman, Y. van der Meer, A. M. van der Kraan, V. H. J. de Beer, J. A. R. van Veen and R. A. van Santen, *J. Catal.*, 2001, **199**, 224-235.
- 82 Y. Romero, F. Richard and S. Brunet, *Appl. Catal. B*, 2010, **98**, 213-223.
- 83 M. C. Daage, R., *J. Catal.*, 1994, **149**, 414-427.
- 84 Y. Q. Yang, C. T. Tye and K. J. Smith, *Catal. Commun.*, 2008, **9**, 1364-1368.
- 85 P. Raybaud, *Appl. Catal. A*, 2007, **322**, 76-91.
- 86 S. Cristol, J. Paul, C. Schovsbo, E. Veilly and E. Payen, *J. Catal.*, 2006, **239**, 145-153.
- 87 V. M. L. Whiffen and K. J. Smith, *Energ. Fuel*, 2010, **24**, 4728-4737.
- 88 W. Wang, S. Tan, K. Wu, G. Zhu, Y. Liu, L. Tan, Y. Huang and Y. Yang, *Fuel*, 2018, **214**, 480-488.
- 89 W. Wang, G. Zhu, L. Li, S. Tan, K. Wu, X. Zhang and Y. Yang, *Fuel*, 2016, **174**, 1-8.
- 90 W. Wang, L. Li, K. Wu, K. Zhang, J. Jie and Y. Yang, *Appl. Catal. A*, 2015, **495**, 8-16.
- 91 W. Song, S. Zhou, S. Hu, W. Lai, Y. Lian, J. Wang, W. Yang, M. Wang, P. Wang and X. Jiang, *ACS Catal.*, 2018, **9**, 259-268.
- 92 B. Yoosuk, D. Tumnantong and P. Prasassarakich, *Chem. Eng. Sci.*, 2012, **79**, 1-7.
- 93 W. Wang, K. Zhang, L. Li, K. Wu, P. Liu and Y. Yang, *Ind. Eng. Chem. Res.*, 2014, **53**, 19001-19009.
- 94 V. N. Bui, D. Laurenti, P. Afanasiev and C. Geantet, *Appl. Catal. B*, 2011, **101**, 239-245.
- 95 V. N. Bui, D. Laurenti, P. Delichère and C. Geantet, *Appl. Catal. B*, 2011, **101**, 246-255.
- 96 T. Viljava, *Catal. Today*, 2000, **60**, 83-92.
- 97 W. Wang, K. Wu, L. Li, S. Tan, G. Zhu, W. Li, Z. He and Y. Yang, *Catal. Commun.*, 2016, **74**, 60-64.
- 98 C. Wang, D. Wang, Z. Wu, Z. Wang, C. Tang and P. Zhou, *Appl. Catal. A*, 2014, **476**, 61-67.
- 99 C. Wang, Z. Wu, C. Tang, L. Li and D. Wang, *Catal. Commun.*, 2013, **32**, 76-80.
- 100 J. N. Shabtai, N.; Massoth, F., *J. Catal.*, 1987, **104**, 413-423.
- 101 W. Wang, L. Li, S. Tan, K. Wu, G. Zhu, Y. Liu, Y. Xu and Y. Yang, *Fuel*, 2016, **179**, 1-9.
- 102 V. Itthibenchapong, C. Ratanatawanate, M. Oura and K. Faungnawakij, *Catal. Commun.*, 2015, **68**, 31-35.
- 103 B. Yoosuk, D. Tumnantong and P. Prasassarakich, *Fuel*, 2012, **91**, 246-252.
- 104 A. Y. Bunch and U. S. Ozkan, *J. Catal.*, 2002, **206**, 177-187.
- 105 A. Y. Bunch, X. Wang and U. S. Ozkan, *J. Mol. Catal. A*, 2007, **270**, 264-272.
- 106 J. Ojeda, N. Escalona, P. Baeza, M. Escudey and F. J. Gil-Llambías, *Chem. Commun.*, 2003, DOI: 10.1039/b301647c, 1608-1609.
- 107 D. K. Lee, I. C. Lee, S. K. Park, S. Y. Bae and S. I. Woo, *J. Catal.*, 1996, **159**, 212-218.
- 108 D. K. Lee, H. T. Lee, I. C. Lee, S. K. Park, S. Y. Bae, C. H. Kim and S. I. Woo, *J. Catal.*, 1996, **159**, 219-229.
- 109 W. Wang, K. Zhang, Z. Qiao, L. Li, P. Liu and Y. Yang, *Catal. Commun.*, 2014, **56**, 17-22.
- 110 V. N. Bui, G. Toussaint, D. Laurenti, C. Mirodatos and C. Geantet, *Catal. Today*, 2009, **143**, 172-178.
- 111 A. Pinheiro, D. Hudebine, N. Dupassieux and C. Geantet, *Energ. Fuel*, 2009, **23**, 1007-1014.
- 112 E. Laurent and B. Delmon, *J. Catal.*, 1994, **146**, 281-291.
- 113 Y. Yoshimura, T. Sato, H. Shimada, N. Matsubayashi and A. Nishijima, *Applied Catalysis*, 1991, **73**, 55-63.
- 114 P. M. Mortensen, D. Gardini, C. D. Damsgaard, J.-D. Grunwaldt, P. A. Jensen, J. B. Wagner and A. D. Jensen, *Appl. Catal. A*, 2016, **523**, 159-170.
- 115 O. İ. Şenol, E. M. Ryymin, T. R. Viljava and A. O. I. Krause, *J. Mol. Catal. A*, 2007, **277**, 107-112.
- 116 A. Gutierrez, E.-M. Turpeinen, T.-R. Viljava and O. Krause, *Catal. Today*, 2017, **285**, 125-134.
- 117 D. D. Laskar, M. P. Tucker, X. Chen, G. L. Helms and B. Yang, *Green Chem.*, 2014, **16**, 897.
- 118 Y. Yoon, R. Rousseau, R. S. Weber, D. Mei and J. A. Lercher, *J. Am. Chem. Soc.*, 2014, **136**, 10287-10298.
- 119 A. J. R. Hensley, Y. Wang and J.-S. McEwen, *Surf. Sci.*, 2016, **648**, 227-235.
- 120 A. J. R. Hensley, Y. Wang and J.-S. McEwen, *ACS Catal.*, 2015, **5**, 523-536.

- 121 Q. Tan, G. Wang, A. Long, A. Dinse, C. Buda, J. Shabaker and D. E. Resasco, *J. Catal.*, 2017, **347**, 102-115.
- 122 M. Shetty, K. Murugappan, T. Prasomsri, W. H. Green and Y. Román-Leshkov, *J. Catal.*, 2015, **331**, 86-97.
- 123 J. Sun, A. M. Karim, H. Zhang, L. Kovarik, X. S. Li, A. J. Hensley, J.-S. McEwen and Y. Wang, *J. Catal.*, 2013, **306**, 47-57.
- 124 Y. Hong, H. Zhang, J. Sun, K. M. Ayman, A. J. R. Hensley, M. Gu, M. H. Engelhard, J.-S. McEwen and Y. Wang, *ACS Catal.*, 2014, **4**, 3335-3345.
- 125 Y. Hong and Y. Wang, *Catal. Commun.*, 2017, **100**, 43-47.
- 126 R. Olcese, M. M. Bettahar, B. Malaman, J. Ghanbaja, L. Tibavizco, D. Petitjean and A. Dufour, *Appl. Catal. B*, 2013, **129**, 528-538.
- 127 Y. Yang, G. Lv, L. Deng, B. Lu, J. Li, J. Zhang, J. Shi and S. Du, *Microporous Mesoporous Mater.*, 2017, **250**, 47-54.
- 128 F. Yang, D. Liu, Y. Zhao, H. Wang, J. Han, Q. Ge and X. Zhu, *ACS Catal.*, 2018, **8**, 1672-1682.
- 129 E.-J. Shin and M. A. Keane, *Ind. Eng. Chem. Res.*, 2000, **39**, 883-892.
- 130 J. E. Peters, J. R. Carpenter and D. C. Dayton, *Energ. Fuel*, 2015, **29**, 909-916.
- 131 P. T. M. Do, A. J. Foster, J. Chen and R. F. Lobo, *Green Chem.*, 2012, **14**, 1388.
- 132 K. A. Resende, A. H. Braga, F. B. Noronha and C. E. Hori, *Appl. Catal. B*, 2019, **245**, 100-113.
- 133 X. Zhang, J. Tang, Q. Zhang, Q. Liu, Y. Li, L. Chen, C. Wang and L. Ma, *Catal. Today*, 2019, **319**, 41-47.
- 134 S. Boullousa-Eiras, R. Lødeng, H. Bergem, M. Stöcker, L. Hannevold and E. A. Blekkan, *Catal. Today*, 2014, **223**, 44-53.
- 135 T. He, X. Liu, Y. Ge, D. Han, J. Li, Z. Wang and J. Wu, *Catal. Commun.*, 2017, **102**, 127-130.
- 136 R. N. Olcese, G. Lardier, M. Bettahar, J. Ghanbaja, S. Fontana, V. Carre, F. Aubriet, D. Petitjean and A. Dufour, *ChemSusChem*, 2013, **6**, 1490-1499.
- 137 P.-J. Hsu, J.-W. Jiang and Y.-C. Lin, *ACS Sustain. Chem. Eng.*, 2017, **6**, 660-667.
- 138 K. Murugappan, E. M. Anderson, D. Teschner, T. E. Jones, K. Skorupska and Y. Román-Leshkov, *Nat. Catal.*, 2018, **1**, 960-967.
- 139 C.-c. Chiu, A. Genest, A. Borgna and N. Rösch, *ACS Catal.*, 2014, **4**, 4178-4188.
- 140 G. Li, J. Han, H. Wang, X. Zhu and Q. Ge, *ACS Catal.*, 2015, **5**, 2009-2016.
- 141 K. Lee, G. H. Gu, C. A. Mullen, A. A. Boateng and D. G. Vlachos, *ChemSusChem*, 2015, **8**, 315-322.
- 142 H. Liu, T. Jiang, B. Han, S. Liang and Y. Zhou, *Science*, 2009, **326**, 1250-1252.
- 143 A. Bjelić, M. Grilc and B. Likozar, *Chem. Eng. J.*, 2018, **333**, 240-259.
- 144 J. Zakzeski, P. C. Bruijninx, A. L. Jongerius and B. M. Weckhuysen, *Chem. Rev.*, 2010, **110**, 3552-3599.
- 145 W. Jin, L. Pastor-Pérez, D. Shen, A. Sepúlveda-Escribano, S. Gu and T. Ramirez Reina, *ChemCatChem*, 2019, **11**, 924-960.
- 146 M. B. Griffin, G. A. Ferguson, D. A. Ruddy, M. J. Bidy, G. T. Beckham and J. A. Schaidle, *ACS Catal.*, 2016, **6**, 2715-2727.
- 147 C. Zhao, J. He, A. A. Lemonidou, X. Li and J. A. Lercher, *J. Catal.*, 2011, **280**, 8-16.
- 148 C. Zhao, Y. Kou, A. A. Lemonidou, X. Li and J. A. Lercher, *Angew. Chem. Int. Ed.*, 2009, **48**, 3987-3990.
- 149 P. M. Mortensen, J.-D. Grunwaldt, P. A. Jensen and A. D. Jensen, *ACS Catal.*, 2013, **3**, 1774-1785.
- 150 H. Wan, R. V. Chaudhari and B. Subramaniam, *Top. Catal.*, 2012, **55**, 129-139.
- 151 D. Shi, L. Arroyo-Ramírez and J. M. Vohs, *J. Catal.*, 2016, **340**, 219-226.
- 152 C. Newman, X. Zhou, B. Goundie, I. T. Ghampson, R. A. Pollock, Z. Ross, M. C. Wheeler, R. W. Meulenberg, R. N. Austin and B. G. Frederick, *Appl. Catal. A*, 2014, **477**, 64-74.
- 153 Q. Tan, G. Wang, L. Nie, A. Dinse, C. Buda, J. Shabaker and D. E. Resasco, *ACS Catal.*, 2015, **5**, 6271-6283.
- 154 G. Yao, G. Wu, W. Dai, N. Guan and L. Li, *Fuel*, 2015, **150**, 175-183.
- 155 Y. Shao, Q. Xia, L. Dong, X. Liu, X. Han, S. F. Parker, Y. Cheng, L. L. Daemen, A. J. Ramirez-Cuesta, S. Yang and Y. Wang, *Nat. Commun.*, 2017, **8**, 16104.
- 156 Y.-B. Huang, L. Yan, M.-Y. Chen, Q.-X. Guo and Y. Fu, *Green Chem.*, 2015, **17**, 3010-3017.
- 157 R. C. Nelson, B. Baek, P. Ruiz, B. Goundie, A. Brooks, M. C. Wheeler, B. G. Frederick, L. C. Grabow and R. N. Austin, *ACS Catal.*, 2015, **5**, 6509-6523.
- 158 Z. Zheng, Z. Luo and C. Zhao, *ChemCatChem*, 2018, **10**, 1376-1384.
- 159 T. N. Phan and C. H. Ko, *Catal. Today*, 2018, **303**, 219-226.
- 160 P. M. de Souza, R. C. Rabelo-Neto, L. E. P. Borges, G. Jacobs, B. H. Davis, T. Sooknoi, D. E. Resasco and F. B. Noronha, *ACS Catal.*, 2015, **5**, 1318-1329.
- 161 A. M. Barrios, C. A. Teles, P. M. de Souza, R. C. Rabelo-Neto, G. Jacobs, B. H. Davis, L. E. P. Borges and F. B. Noronha, *Catal. Today*, 2018, **302**, 115-124.
- 162 Q. Lai, C. Zhang and J. H. Holles, *Appl. Catal. A*, 2016, **528**, 1-13.
- 163 X. Zhu, L. Nie, L. L. Lobban, R. G. Mallinson and D. E. Resasco, *Energ. Fuel*, 2014, **28**, 4104-4111.
- 164 X. Zhu, L. L. Lobban, R. G. Mallinson and D. E. Resasco, *J. Catal.*, 2011, **281**, 21-29.
- 165 L. Nie, B. Peng and X. Zhu, *ChemCatChem*, 2018, **10**, 1064-1074.
- 166 C. Wang, A. V. Mironenko, A. Raizada, T. Q. Chen, X. Y. Mao, A. Padmanabhan, D. G. Vlachos, R. J. Gorte and J. M. Vohs, *ACS Catal.*, 2018, **8**, 7749-7759.
- 167 M. A. n. González-Borja and D. E. Resasco, *Energ. Fuel*, 2011, **25**, 4155-4162.
- 168 I. T. Ghampson, C. Sepúlveda, R. García, J. L. G. Fierro and N. Escalona, *Catal. Sci. Technol.*, 2016, **6**, 4356-4369.
- 169 I. T. Ghampson, G. Pecchi, J. L. G. Fierro, A. Videla and N. Escalona, *Appl. Catal. B*, 2017, **208**, 60-74.
- 170 I. T. Ghampson, R. Canales and N. Escalona, *Appl. Catal. A*, 2018, **549**, 225-236.
- 171 P. Sirous-Rezaei, J. Jae, K. Cho, C. H. Ko, S.-C. Jung and Y.-K. Park, *Chem. Eng. J.*, 2018, DOI: 10.1016/j.cej.2018.10.058.
- 172 A. J. R. Hensley, Y. Hong, R. Zhang, H. Zhang, J. Sun, Y. Wang and J.-S. McEwen, *ACS Catal.*, 2014, **4**, 3381-3392.
- 173 K. P. Kepp, *Inorg Chem*, 2016, **55**, 9461-9470.
- 174 S. T. Oyama, T. Gott, H. Zhao and Y.-K. Lee, *Catal. Today*, 2009, **143**, 94-107.
- 175 Q. Chang, C. Zhang, C. Liu, Y. Wei, A. V. Cheruvathur, A. I. Dugulan, J. W. Niemantsverdriet, X. Liu, Y. He, M. Qing, L. Zheng, Y. Yun, Y. Yang and Y. Li, *ACS Catal.*, 2018, **8**, 3304-3316.
- 176 R. Kojima and K.-i. Aika, *Appl. Catal. A*, 2001, **219**, 141-147.
- 177 G. Shi, L. Su and K. Jin, *Catal. Commun.*, 2015, **59**, 180-183.
- 178 E. de Smit and B. M. Weckhuysen, *Chem. Soc. Rev.*, 2008, **37**, 2758.
- 179 R. B. Levy and M. Boudart, *Science*, 1973, **181**, 547-549.
- 180 S. T. Oyama, *J. Catal.*, 2003, **216**, 343-352.
- 181 J. S. J. Hargreaves, *Coord. Chem. Rev.*, 2013, **257**, 2015-2031.

- 182 J. Pang, J. Sun, M. Zheng, H. Li, Y. Wang and T. Zhang, *Appl. Catal. B*, 2019, **254**, 510-522.
- 183 S. Ramanathan and S. T. Oyama, *J. Phys. Chem.*, 1995, **99**, 16365-16372.
- 184 W. R. A. M. Robinson, J. N. M. van Gestel, T. I. Korányi, S. Eijssbouts, A. M. van der Kraan, J. A. R. van Veen and V. H. J. de Beer, *J. Catal.*, 1996, **161**, 539-550.
- 185 P. Clark, Oyama, S., *J. Catal.*, 2003, **218**, 78-87.
- 186 E. Furimsky, *Appl. Catal. A*, 2003, **240**, 1-28.
- 187 Z. Lin, R. Chen, Z. Qu and J. G. Chen, *Green Chem.*, 2018, **20**, 2679-2696.
- 188 C. Chan-Thaw and A. Villa, *Appl. Sci.*, 2018, **8**, 259.
- 189 M. M. Sullivan, C.-J. Chen and A. Bhan, *Catal. Sci. Technol.*, 2016, **6**, 602-616.
- 190 P. Bui, J. A. Cecilia, S. T. Oyama, A. Takagaki, A. Infantes-Molina, H. Zhao, D. Li, E. Rodríguez-Castellón and A. Jiménez López, *J. Catal.*, 2012, **294**, 184-198.
- 191 H. Y. Zhao, D. Li, P. Bui and S. T. Oyama, *Appl. Catal. A*, 2011, **391**, 305-310.
- 192 A. Berenguer, T. M. Sankaranarayanan, G. Gómez, I. Moreno, J. M. Coronado, P. Pizarro and D. P. Serrano, *Green Chem.*, 2016, **18**, 1938-1951.
- 193 Y. Lee and S. Oyama, *J. Catal.*, 2006, **239**, 376-389.
- 194 J. Monnier, H. Sulimma, A. Dalai and G. Caravaggio, *Appl. Catal. A*, 2010, **382**, 176-180.
- 195 W.-S. Lee, Z. Wang, R. J. Wu and A. Bhan, *J. Catal.*, 2014, **319**, 44-53.
- 196 C.-J. Chen, W.-S. Lee and A. Bhan, *Appl. Catal. A*, 2016, **510**, 42-48.
- 197 W.-S. Lee, A. Kumar, Z. Wang and A. Bhan, *ACS Catal.*, 2015, **5**, 4104-4114.
- 198 C.-J. Chen and A. Bhan, *ACS Catal.*, 2017, **7**, 1113-1122.
- 199 H. Wang, S. Liu and K. J. Smith, *Energ. Fuel*, 2016, **30**, 6039-6049.
- 200 Q. Lu, C.-J. Chen, W. Luc, J. G. Chen, A. Bhan and F. Jiao, *ACS Catal.*, 2016, **6**, 3506-3514.
- 201 A. A. Smirnov, Z. Geng, S. A. Khromova, S. G. Zavarukhin, O. A. Bulavchenko, A. A. Saraev, V. V. Kaichev, D. Y. Ermakov and V. A. Yakovlev, *J. Catal.*, 2017, **354**, 61-77.
- 202 T. Iida, M. Shetty, K. Murugappan, Z. Wang, K. Ohara, T. Wakihara and Y. Román-Leshkov, *ACS Catal.*, 2017, **7**, 8147-8151.
- 203 J.-S. Moon, E.-G. Kim and Y.-K. Lee, *J. Catal.*, 2014, **311**, 144-152.
- 204 X. Lan, E. J. M. Hensen and T. Weber, *Appl. Catal. A*, 2018, **550**, 57-66.
- 205 Y. Li, J. Fu and B. Chen, *RSC Adv.*, 2017, **7**, 15272-15277.
- 206 V. M. L. Whiffen, K. J. Smith and S. K. Straus, *Appl. Catal. A*, 2012, **419-420**, 111-125.
- 207 C. Sepúlveda, K. Leiva, R. García, L. R. Radovic, I. T. Ghampson, W. J. DeSisto, J. L. G. Fierro and N. Escalona, *Catal. Today*, 2011, **172**, 232-239.
- 208 I. T. Ghampson, C. Sepúlveda, R. García, L. R. Radovic, J. L. G. Fierro, W. J. DeSisto and N. Escalona, *Appl. Catal. A*, 2012, **439-440**, 111-124.
- 209 I. T. Ghampson, C. Sepúlveda, R. García, B. G. Frederick, M. C. Wheeler, N. Escalona and W. J. DeSisto, *Appl. Catal. A*, 2012, **413-414**, 78-84.
- 210 I. Tyrone Ghampson, C. Sepúlveda, R. García, J. L. García Fierro, N. Escalona and W. J. DeSisto, *Appl. Catal. A*, 2012, **435-436**, 51-60.
- 211 J. A. Cecilia, A. Infantes-Molina, E. Rodríguez-Castellón, A. Jiménez-López and S. T. Oyama, *Appl. Catal. B*, 2013, **136-137**, 140-149.
- 212 D. J. Rensel, J. Kim, Y. Bonita and J. C. Hicks, *Appl. Catal. A*, 2016, **524**, 85-93.
- 213 Y. Li, C. Zhang, Y. Liu, S. Tang, G. Chen, R. Zhang and X. Tang, *Fuel*, 2017, **189**, 23-31.
- 214 T. Bligaard and J. K. Nørskov, *Electrochim. Acta*, 2007, **52**, 5512-5516.
- 215 V. O. O. Gonçalves, P. M. de Souza, V. T. da Silva, F. B. Noronha and F. Richard, *Appl. Catal. B*, 2017, **205**, 357-367.
- 216 Z. Yu, Y. Wang, Z. Sun, X. Li, A. Wang, D. M. Camaioni and J. A. Lercher, *Green Chem.*, 2018, **20**, 609-619.
- 217 X. Liu, L. Xu, G. Xu, W. Jia, Y. Ma and Y. Zhang, *ACS Catal.*, 2016, **6**, 7611-7620.
- 218 C. Zhao and J. A. Lercher, *Angew. Chem. Int. Ed.*, 2012, **51**, 5935-5940.
- 219 H. Fang, A. Roldan, C. Tian, Y. Zheng, X. Duan, K. Chen, L. Ye, S. Leoni and Y. Yuan, *J. Catal.*, 2019, **369**, 283-295.
- 220 K. A. Goulas, A. V. Mironenko, G. R. Jenness, T. Mazal and D. G. Vlachos, *Nat. Catal.*, 2019, **2**, 269-276.
- 221 H. Yan, H. Cheng, H. Yi, Y. Lin, T. Yao, C. Wang, J. Li, S. Wei and J. Lu, *J. Am. Chem. Soc.*, 2015, **137**, 10484-10487.
- 222 X. Li, W. Bi, L. Zhang, S. Tao, W. Chu, Q. Zhang, Y. Luo, C. Wu and Y. Xie, *Adv. Mater.*, 2016, **28**, 2427-2431.
- 223 X. I. Pereira-Hernandez, A. DeLaRiva, V. Muravev, D. Kunwar, H. Xiong, B. Sudduth, M. Engelhard, L. Kovarik, E. J. M. Hensen, Y. Wang and A. K. Datye, *Nat. Commun.*, 2019, **10**, 1358.
- 224 C. Zhang, C. Jia, Y. Cao, Y. Yao, S. Xie, S. Zhang and H. Lin, *Green Chem.*, 2019, **21**, 1668-1679.
- 225 G.-H. Liu, Z.-M. Zong, Z.-Q. Liu, F.-J. Liu, Y.-Y. Zhang and X.-Y. Wei, *Fuel Process. Technol.*, 2018, **179**, 114-123.
- 226 Z. Zhao, R. Bababrik, W. Xue, Y. Li, N. M. Briggs, D.-T. Nguyen, U. Nguyen, S. P. Crossley, S. Wang, B. Wang and D. E. Resasco, *Nat. Catal.*, 2019, **2**, 431-436.
- 227 A. G. Sergeev and J. F. Hartwig, *Science*, 2011, **332**, 439-443.
- 228 F. Gao, J. D. Webb and J. F. Hartwig, *Angew. Chem. Int. Ed.*, 2016, **55**, 1474-1478.
- 229 Y. Ren, M. Yan, J. Wang, Z. C. Zhang and K. Yao, *Angew. Chem. Int. Ed.*, 2013, **125**, 12906-12910.
- 230 J. Sun, A. M. Karim, X. S. Li, J. Rainbolt, L. Kovarik, Y. Shin and Y. Wang, *Chem. Commun.*, 2015, **51**, 16617-16620.